Article

Cell Reports

Quiescence Exit of Tert+ Stem Cells by Wnt/β-Catenin Is Indispensable for Intestinal Regeneration

Graphical Abstract

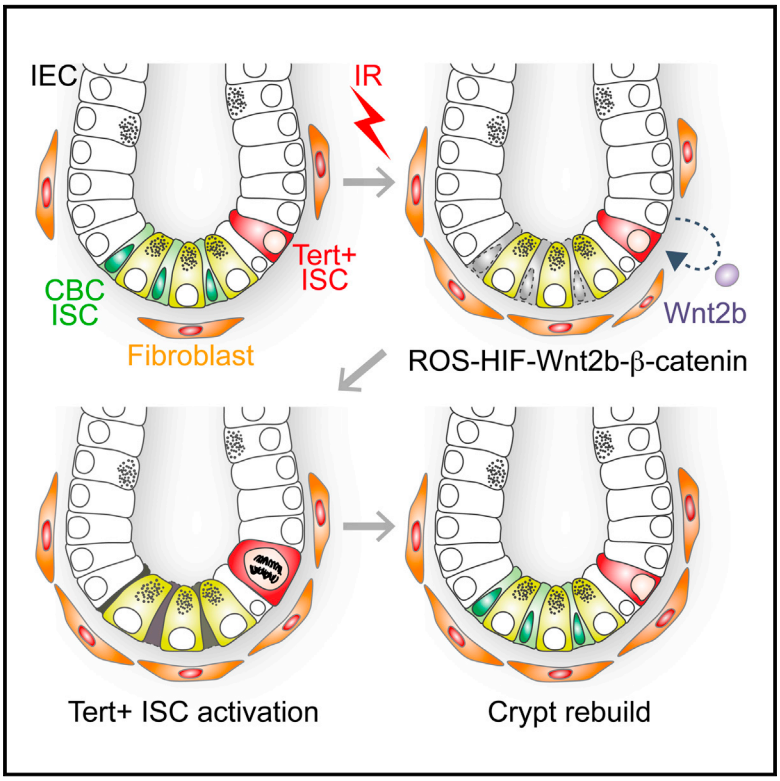

Authors

Han Na Suh, Moon Jong Kim, Youn-Sang Jung, Esther M. Lien, Sohee Jun, Jae-Il Park

Correspondence

jaeil@mdanderson.org

In Brief

Suh et al. define Tert+ cells as stem cells essential for intestinal regeneration and unveil how Tert+ intestinal stem cells escape from the quiescent state and undergo repopulation into progenitor cells upon tissue injury.

Highlights

- Tert+ cells are quiescent but conditionally repopulated upon tissue injury
- Tert+ cells are indispensable for intestinal regeneration
- ROS-HIFs-transactivated *Wnt2b* hyperactivates Wnt signaling in Tert+ cells
- β-catenin induces quiescence exit of Tert+ cells

Suh et al., 2017, Cell Reports *21*, 2571–2584
November 28, 2017
https://doi.org/10.1016/j.celrep.2017.10.118

Cell Reports
Article

Quiescence Exit of Tert$^+$ Stem Cells by Wnt/β-Catenin Is Indispensable for Intestinal Regeneration

Han Na Suh,[1] Moon Jong Kim,[1] Youn-Sang Jung,[1] Esther M. Lien,[1] Sohee Jun,[1] and Jae-Il Park[1,2,3,4,*]
[1]Department of Experimental Radiation Oncology, Division of Radiation Oncology, The University of Texas, MD Anderson Cancer Center, Houston, TX 77030, USA
[2]Graduate School of Biomedical Sciences, The University of Texas, MD Anderson Cancer Center, Houston, TX 77030, USA
[3]Program in Genes and Development, The University of Texas MD, Anderson Cancer Center, Houston, TX 77030, USA
[4]Lead Contact
*Correspondence: jaeil@mdanderson.org
https://doi.org/10.1016/j.celrep.2017.10.118

SUMMARY

Fine control of stem cell maintenance and activation is crucial for tissue homeostasis and regeneration. However, the mechanism of quiescence exit of Tert$^+$ intestinal stem cells (ISCs) remains unknown. Employing a *Tert* knockin (*Tert$^{TCE/+}$*) mouse model, we found that Tert$^+$ cells are long-term label-retaining self-renewing cells, which are partially distinguished from the previously identified +4 ISCs. Tert$^+$ cells become mitotic upon irradiation (IR) injury. Conditional ablation of Tert$^+$ cells impairs IR-induced intestinal regeneration but not intestinal homeostasis. Upon IR injury, Wnt signaling is specifically activated in Tert$^+$ cells via the ROS-HIFs-transactivated *Wnt2b* signaling axis. Importantly, conditional knockout of β-catenin/*Ctnnb1* in Tert$^+$ cells undermines IR-induced quiescence exit of Tert$^+$ cells, which subsequently impedes intestinal regeneration. Our results that Wnt-signaling-induced activation of Tert$^+$ ISCs is indispensable for intestinal regeneration unveil the underlying mechanism for how Tert$^+$ stem cells undergo quiescence exit upon tissue injury.

INTRODUCTION

Stem cells (SCs) are consistently or conditionally activated for tissue homeostasis or regeneration (Barker, 2014). The fine-tuned SC dynamics are governed by both cell intrinsic (Blanpain et al., 2006; Lowell et al., 2000), and cell extrinsic factors (Choi et al., 2013; Lim et al., 2013; Eisenhoffer et al., 2012; Marinari et al., 2012). Intestinal epithelium are composed of heterogeneous cell populations (absorptive enterocytes, secretive goblet cells, enteroendocrine cells, and Paneth cells) that originate from intestinal stem cells (ISCs) and are rapidly replenished from the crypts to the villi (Sancho et al., 2003). Two distinct ISCs co-exist in the crypts (Barker, 2014). While the highly proliferative crypt base columnar (CBC) ISCs (Lgr5$^+$) continuously generate intestinal epithelial cells (IECs) for tissue homeostasis (Snippert et al., 2010), the relatively quiescent position 4 (+4) ISCs, located above the Paneth cells, are involved in intestinal regeneration (Yan et al., 2012).

Several markers of quiescence ISCs with distinct expression patterns have been identified. For example, +4 ISCs are co-localized with Bmi1-expression cells (Yan et al., 2012; Sangiorgi and Capecchi, 2008), whereas *Bmi1* is broadly expressed in the crypt, including the Lgr5$^+$ cells (Itzkovitz et al., 2011; Muñoz et al., 2012). In *Tert* transgenic mouse, Tert$^+$ cells are mainly located in the +5 to +8 position (Montgomery et al., 2011). In addition, proliferative Hopx$^+$ cells are found at +4 after irradiation (IR) (Takeda et al., 2011). Furthermore, quiescent labeled-retaining cells (LRCs) are thought to be the precursor of secretory cells expressing *Lgr5* (Buczacki et al., 2013). Nonetheless, quiescent ISCs need to be further validated given the various expression of Lgr5 in the crypts. To overcome the current technical limitation in studying SCs, we recently generated a *Tert* knockin mouse model (Jun et al., 2016). Tert, a catalytic subunit of telomerase, is specifically expressed in self-renewing cells including SCs, germ cells, and cancer cells (Flores et al., 2006). By utilizing Tert expression as a functional SC marker in our study, here, we explore the biology of Tert$^+$ SCs in tissue regeneration.

High-dose ionizing radiation induces the loss of crypt cells, resulting in radiation-induced gastrointestinal syndrome (RIGS) (Saha et al., 2011). Owing to damaged stem cell population in the crypts, RIGS prevents the replenishment of intestinal epithelium and leads to several pathophysiological conditions including electrolyte imbalance, diarrhea, and weight loss (Zimmerer et al., 2008). Recent therapeutic strategies for RIGS are transplantation of stromal cells (Saha et al., 2011), treatment with R-spondin 1 (Bhanja et al., 2009), or administration of macrophage-derived WNTs (Saha et al., 2016), suggesting that Wnt/β-catenin signaling might be essential for tissue regeneration. Herein, we will dissect the mechanism of how ISCs are activated during intestinal regeneration.

RESULTS

Conditional Repopulation of Tert$^+$ Cells upon Radiation Injury

A *Tert* knockin mouse (hereafter referred as *Tert$^{TCE/+}$*) expresses tdTomato-CreERT2 (TCE) driven by the endogenous *Tert*

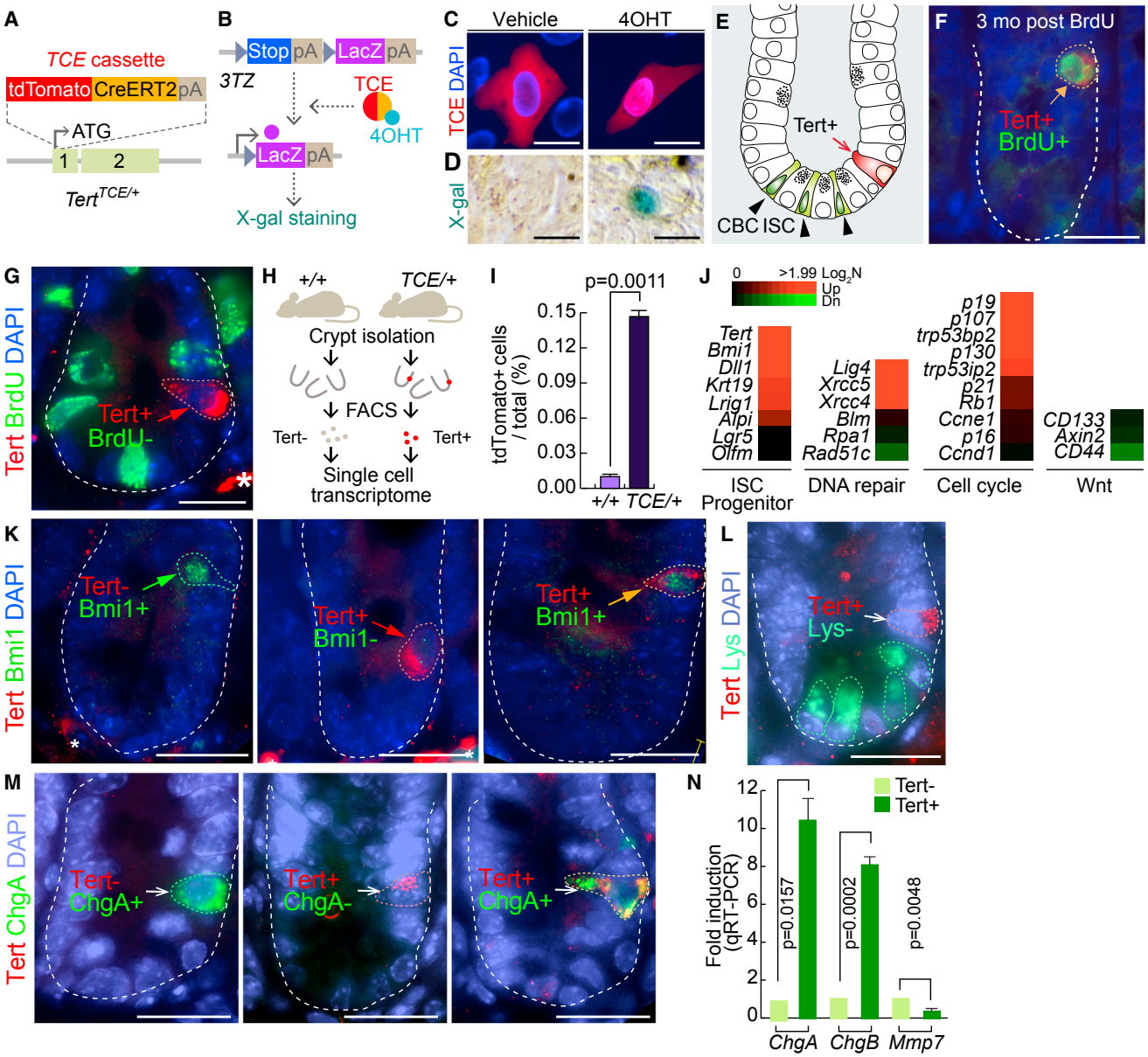

Figure 1. Characterization of Tert$^+$ Cells in the Intestine

(A) Generation of the *Tert*$^{TCE/+}$ knockin mouse model by gene targeting. A tdTomato-CreERT2 (TCE) cassette was inserted in-frame into the *Tert* allele.

(B) Conditional activation of TCE by 4-hydroxytamoxifen (4OHT). 3TZ cells were transfected with a TCE-expressing plasmid. 4OHT-activated TCE induces Cre-loxP recombination, resulting in expression of LacZ, detected by β-galactosidase (X-gal) staining.

(C) Nuclear translocation of TCE by 4-OHT. HeLa cells were transfected with TCE plasmid and treated with 4OHT (100 μM for 24 hr). Scale bars, 20 μm.

(D) TCE-induced Cre-LoxP recombination by 4-OHT. 3TZ cells were transfected with TCE plasmid, treated with 4OHT (100 μM for 36 hr), and visualized by β-galactosidase (X-gal) staining. Scale bars, 20 μm.

(E) Illustration of ISCs and Tert$^+$ cells in the small intestine. Tert$^+$ cells are located at position 4 (+4) (arrow), and the crypt base columnar (CBC) ISCs are located at the bottom of crypts (arrowheads).

(F) Label-retaining cell assay. *Tert*$^{TCE/+}$ mice (2 weeks of age) were injected with BrdU, and tissue was collected at 3 months of age. Tert$^+$:BrdU$^+$ cell is indicated by an arrow. Scale bars, 20 μm.

(G) Bromodeoxyuridine (BrdU) incorporation assay. Briefly, *Tert*$^{TCE/+}$ mice were injected with BrdU (1 mg in PBS) 30 min before tissue collection, and the small intestine was subjected to IF staining. Tert$^+$:BrdU$^-$ cells are indicated by an arrow. An asterisk indicates a non-specific signal. Scale bars, 20 μm.

(H and I) Isolation and validation of Tert$^+$ cells using fluorescence-activated cell sorting (FACS) (H) and qRT-PCR (I).

(J) Single-cell gene expression profiling of Tert$^+$ cells compared to Tert$^-$ cells.

(K) Tert$^+$ cells partially overlap with Bmi1$^+$ cells in the small intestine.

(L) Tert$^+$ cells do not overlap with lysozyme$^+$ cells (Paneth cell) in the small intestine.

(legend continued on next page)

promoter (Jun et al., 2016) (Figure 1A). We first tested whether the TCE protein conditionally induces Cre-loxP recombination. Tamoxifen (Tam) treatment induced the nuclear translocation of TCE protein and subsequent Cre-loxP recombination, represented by LacZ expression in 3TZ, Cre-loxP recombination reporter cells (Psarras et al., 2004) (Figures 1B–1D). Employing *Tert*$^{TCE/+}$ mice, we found that Tert^{+} cells resided at the +3∼+4 position beyond CBC ISCs in the intestine, at a frequency of one Tert^{+} cell per 120.5 ± 26.50 crypts (Figures 1E and S1A). To determine whether Tert^{+} cells are quiescent ISCs, we performed a label-retaining cell (LRC) assay by a single-dose injection of bromodeoxyuridine (BrdU) into *Tert*$^{TCE/+}$ mice (Hsu and Fuchs, 2012; Potten et al., 2002). 3 months after BrdU administration, we detected Tert^{-}:BrdU^{+} (20.6%), Tert^{+}:BrdU^{-} (43%), and Tert^{+}:BrdU^{+} (36.4%) in the crypts (Figures 1F and S1C), suggesting that some Tert^{+} cells are long-term LRCs. Consistently, BrdU incorporation assays (BrdU injection 0.5 hr prior to tissue collection) showed that Tert^{+} cells were not proliferative in the homeostatic intestine (Figure 1G). Next, we performed single-cell gene expression analysis of Tert^{+} cells isolated from the intestinal crypt using fluorescence-activated cell sorting (FACS) (Figures 1H, 1I, and S1B). Tert^{+} cells exhibited the prominent enrichment for *Tert* and *Bmi1* expression (Figure 1J); however, immunofluorescent (IF) staining shows that not all Tert^{+} cells are Bmi1^{+} cells (Figures 1K and S1D). The progenitor cell markers (*Dll1*, *Krt19*, *Lrig1*, and *Alpi*) and non-homologous end-joining DNA repair components (*Lig4*, *Xrcc5*, and *Xrcc4*) were also upregulated in Tert^{+} cells, whereas the expression of homologous recombination DNA repair-related genes (*Blm*, *Rpa1*, and *Rad51c*) did not show any difference between Tert^{+} and Tert^{-} cells. Interestingly, Tert^{+} cells exhibited the high expression of cell-cycle arrest-related genes (*p19*, *p107*, *p53*, *p130*, and *p21*), but no change in Wnt target gene expression (*CD133*, *Axin2*, and *CD44*) compared to Tert^{-} cells (Figure 1J). These results support that Tert^{+} cells are long-term LRCs. Previously, it was reported that LRCs are secretory precursor cells (Buczacki et al., 2013). To determine whether Tert^{+} long-term LRCs share similar markers as secretory precursor cells, we performed immunohistochemistry (IHC) for detecting the Paneth cells or enteroendocrine cells. We found that Tert^{+} cells are not co-localized with lysozyme^{+} cells (the Paneth cell) (Figures 1L and S1E). Intriguingly, we located a few ChgA^{+} cells in the crypts as Tert^{+} cells (Figures 1M and S1F). These results were also confirmed by measuring the expression of *ChgA*, *ChgB*, and *Mmp7* in Tert^{+} cells by qRT-PCR. Compared to Tert^{-} cells, Tert^{+} cells displayed an increase of enteroendocrine cell marker genes (*ChgA*, *ChgB*), whereas no enrichment of the Paneth cell marker gene (*Mmp7*) in Tert^{+} cells was detected (Figure 1N). These results suggest that a small portion of Tert^{+} cells includes enteroendocrine precursor cells, but not Paneth cells, a finding that partially supports the previous study (Buczacki et al., 2013).

Given the specific expression of Tert in self-renewing cells (Hiyama and Hiyama, 2007), we hypothesized that Tert^{+} cells are quiescent ISCs but conditionally repopulated upon tissue injury. To test this, mice were exposed to whole-body irradiation (WBI; 10 Gy) for injury and monitored for intestinal regeneration. After ionizing radiation (IR), proliferating cells (transit-amplifying and CBC cells) were depleted mainly due to DNA damage and apoptosis (Figures 2A–2C, S2A, and S2B). Interestingly, despite the massive depletion of IECs by IR, *Tert* mRNA was markedly upregulated in the crypt, implying the increase of Tert^{+} cells and/or *Tert* mRNA during regeneration (Figure 2D). To clarify this, we determined whether IR induces proliferation of Tert^{+} cells. While Tert^{+} cells were non-proliferative (Tert^{+}:Ki67^{-}) during intestinal homeostasis, Tert^{+} cells became proliferative after IR (Figures 2E–2H). The number of proliferative Tert^{+} cells was increased until 2 dpi (days post injury) (more than 4-fold) and restored at 4 dpi (Figure 2G). Single-cell gene expression analysis of Tert^{+} cells at 1 dpi showed an increase of *Cyclin D1* and *c-Myc* expression but decreased expression of *p21* (Figure 2I), supporting the notion that IR induces the proliferation of Tert^{+} cells. Next, we asked whether mitotically activated Tert^{+} cells generate IECs by employing lineage-tracing assay. *Tert*$^{TCE/+}$*:R26eYFP* strain treated with Tam and IR exhibited repopulation of Tert^{+} cells into IECs during regeneration (Figure 2J). Furthermore, given the co-existence of proliferative (Lgr5^{+}) and quiescent (+4) ISCs in the intestinal crypts, we assessed the cell population kinetics between Tert^{+} cells and Lgr5^{+} ISCs during intestinal regeneration. Upon IR injury, most Lgr5^{+} cells were depleted at 1 dpi and then recovered through 7 dpi. Conversely, Tert^{+} cells were markedly increased until 2 dpi and returned to the basal level at 7 dpi (Figures 2K and S2C). Intriguingly, *Lgr5* mRNA expression in Tert^{+} cells was significantly elevated at 1 dpi (Figure 2L) and the progeny of Tert^{+} cells (YFP^{+}) were found between the Paneth cells at the bottom of the crypt (Figure 2M). These results imply that Tert^{+} cells might serve as a reservoir for Lgr5^{+} cells during intestinal regeneration.

To be defined as SCs, SCs should repopulate into progenitor cells and self-renew. Having observed the repopulation of Tert^{+} cells into IECs by injury (Figures 2J and 2M), we next asked whether Tert^{+} cells are activated by successive injuries. We treated *Tert*$^{TCE/+}$ mice with sequential IR injuries (6 Gy, nonlethal dose but sufficient to induce intestinal injury) to label the dividing cells along with the simultaneous injection of thymidine analogs (IdU for the first round of injury and CldU for the second round of injury) (Figures 2N–2P). We found that Tert^{+} cells were labeled with both IdU and CldU after two consecutive regenerations (28 days later) (Figure 2P). Of note, due to the rapid replenishment of intestinal epithelium (3–5 days), only LRCs remain with IdU or CldU labeling. These results further suggest that Tert^{+} cells are quiescent ISCs, which are conditionally repopulated into IECs during intestinal regeneration.

(M) Tert^{+} cells partially overlap with ChgA^{+} cells (enteroendocrine cell) in the small intestine.
IHC of Tert-:Bmi1^{+}, Tert^{+}:Bmi1^{-}, Tert^{+}:Bmi1^{+}, Tert^{+}:Lysozyme-, Tert^{-}:ChgA^{+}, Tert^{+}:ChgA^{-}, Tert^{+}:ChgA^{+} cells from the *Tert*$^{TCE/+}$ mice. Scale bars, 20 μm.
(N) Expression of *ChgA*, *ChgB*, and *Mmp7* in Tert^{+} cells.
Tert^{+} cells were isolated from *Tert*$^{TCE/+}$ mice and markers for Paneth and enteroendocrine cells were assessed by qRT-PCR. Tert^{-} cells were used as the control sample. Error bars indicate SEM.
The representative images are shown; N ≥ 3.

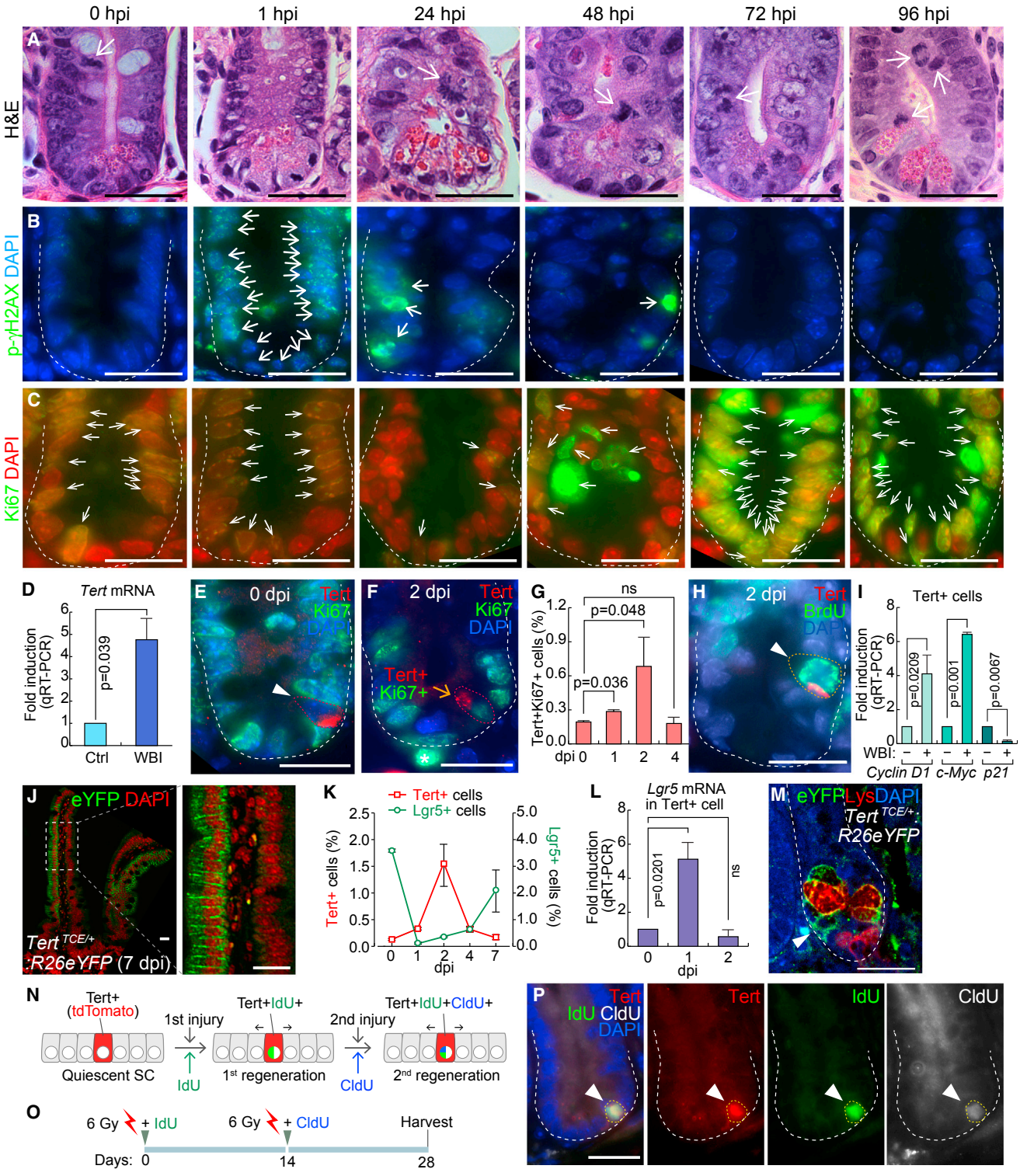

Figure 2. Quiescence Exit of Tert$^+$ Cells upon Radiation Injury

(A–C) Regeneration of intestinal crypt upon IR injury. Mice (5 weeks) were treated with whole-body irradiation (WBI; 10 Gy; a single dose). H&E staining (A); DNA damage foci (phospho-gamma histone H2AX) (B); and proliferation (Ki67) (C). hpi, hour post-injury. Scale bars, 20 μm.

(D) *Tert* mRNA upregulation in the crypts after WBI (10 Gy). qRT-PCR of intestinal crypts at 24 hpi.

(E) Quiescence of Tert$^+$ cells during intestinal homeostasis. Tert$^+$:Ki67$^-$ cells (arrowhead) of *Tert*$^{TCE/+}$ mice. dpi, day post-injury. Scale bars, 20 μm.

(legend continued on next page)

Impaired Intestinal Regeneration by Conditional Ablation of Tert$^+$ Cells

Having determined the quiescence exit of Tert$^+$ cells upon intestinal injury, we next asked whether Tert$^+$ cells are indispensable for intestinal regeneration. To address this, we generated a *Tert$^{TCE/+}$:R26DTA* compound strain. Upon Tam administration, diphtheria toxin A (DTA) is specifically expressed in Tert$^+$ cells, which leads to their selective removal by cell death (about 70% removal of Tert$^+$ cells) (Figures 3A, 3B, S3A, and S3B). Before cell ablation experiments, we tested whether *de novo* generation of Tert$^+$ cells occurs. *Tert$^{TCE/+}$:R26DTA* mice were injected with Tam to deplete Tert$^+$ cells and assessed for Tert$^+$ cells using FACS. We found that Tert$^+$ cells were not generated up to 30 days after Tam administration, which excludes the potential *de novo* generation of Tert$^+$ cells in our experimental setting (Figures S4A and S4B). Next, we asked whether removal of Tert$^+$ cells impairs intestinal regeneration. Intriguingly, *Tert$^{TCE/+}$:R26DTA* strain treated with Tam and IR (experimental group) showed the significant loss of intestinal epithelium integrity, decreased proliferation, and increased apoptosis in IECs of the crypts (Figures 3C–3G and S4C). It is noteworthy that other control groups without IR (*Tert$^{+/+}$* and *Tert$^{TCE/+}$:R26DTA* treated with Tam) displayed no defects in intestinal homeostasis (Figures S3C–S3J), indicating that Tert$^+$ cells are not essential for normal intestinal homeostasis. Additionally, upon Tert$^+$ cell ablation followed by IR, the intestinal epithelium showed abnormal lineage development of the Paneth cell, goblet cell, enterocyte, and enteroendocrine cell throughout the villi and crypts (Figures 3H–3K) as well as the increased mouse mortality (Figure S3K). These results suggest that Tert$^+$ cells are indispensable for intestinal regeneration.

IR-Activated Wnt/β-Catenin Signaling in Tert$^+$ Cells via Reactive Oxygen Species-Hypoxia-Inducible Factors-Wnt2b

Next, we sought to dissect how tissue injury triggers the quiescence exit of Tert$^+$ cells for intestinal regeneration. To identify specific signaling pathway(s) involved in Tert$^+$ ISC activation, we performed gene expression analysis of several candidate signaling pathway target genes. We found that IR markedly upregulated Wnt target genes (*CD44*, *CD133*, and *Axin2*) in the crypts (Figure 4A), which was further confirmed by the increase of β-catenin reporter activity (X-gal staining of *Axin2-LacZ* mice), β-catenin protein, and β-catenin target gene expression (CD44 and Cyclin D1) (Figures 4B–4E and S5A). These results suggest that IR activates Wnt/β-catenin signaling in the crypts, which implies the possible involvement of Wnt signaling in Tert$^+$ ISC activation.

Given the pivotal roles of Wnt ligands and agonists in the maintenance of intestinal integrity via β-catenin-mediated gene regulation (Farin et al., 2012; Kim et al., 2005), we hypothesized that IR-induced upregulation of Wnt ligands triggers target gene activation. To test this, we assessed the expression of nineteen Wnt ligands in the crypt (±IR). We found that *Wnt2b*, *Wnt4*, *Wnt5a*, *Wnt6*, *Wnt7b*, and *Wnt9a* were upregulated by IR (Figures 4F and S5B). To further examine the localization and expression pattern of these Wnt ligands, we performed fluorescence *in situ* hybridization (FISH). Among the six Wnt ligands selected, *Wnt2b* expression was the most prominently upregulated in the intestinal epithelial cells of the crypts after IR (Figure 4H). We found that *Wnt4* is specifically expressed in the mesenchyme during intestinal homeostasis (non-IR treated) and in the epithelium during regeneration (IR treated) (Figure S5E). *Wnt5a* was found expressed at the crypt-villus junction while *Wnt6* and *Wnt9a* were expressed in the crypt in both normal and regenerating intestine (Figures S5F, S5G, and S5I). Lastly, *Wnt7b*-expressing cells were localized in the mesenchyme and were slightly upregulated by IR (Figure S5H). Upregulation of Wnt ligands from our semiquantitative RT-PCR might be due to either transcriptional upregulation or increase of expressing cells. It is noteworthy that we observed an increased frequency of *Wnt5a*, *Wnt6*, or *Wnt9a*-expressing cells after IR, but not their transcriptional upregulation (Figures S5J and S5K). However, *Wnt2b* was the most significantly upregulated by IR at the transcriptional level and the increase of Wnt2b-expressing cells (Figure 4H). In the normal intestine, Wnt2b is expressed in the mesenchymal fibroblasts near the crypts (Valenta et al., 2016) (Figures 4G–4H). To exclude the involvement of Wnt2b secreted from the mesenchymal cells, we isolated and cultured crypt IECs for the crypt organoid development and the subsequent IR treatment. FISH for Wnt2b showed that IR conditionally activated the *Wnt2b* expression in the mesenchymal cell-free crypt organoids (Figure 4I).

(F) Activation of Tert$^+$ cells during regeneration (10 Gy, 2 dpi). Tert$^+$:Ki67$^+$ cells (arrow) of *Tert$^{TCE/+}$* mice. Scale bar, 20 μm.
(G) Quiescence exit of Tert$^+$ cells by WBI. *Tert$^{TCE/+}$* mice treated with WBI (10 Gy) were collected (0, 1, 2, and 4 dpi) to assess Tert$^+$:Ki67$^+$ cells using FACS.
(H) Mitotic activation of Tert$^+$ cells by WBI. *Tert$^{TCE/+}$* mice were treated with WBI (10 Gy). At 2 dpi, BrdU (1 mg/mL, i.p.) was administrated 30 min before tissue collection, and the small intestine was subjected to IF staining. Tert$^+$:BrdU$^+$ cells (arrowhead). Scale bars, 20 μm.
(I) Expression of cell-cycle-related genes in Tert$^+$ cells. *Tert$^{TCE/+}$* mice were treated with WBI (10 Gy, 24 hpi) and subjected to Tert$^+$ cell isolation from intestinal crypts using FACS and qRT-PCR for *Cyclin D1*, *c-Myc*, and *p21* expression.
(J) Lineage tracing of Tert$^+$ cells. *Tert$^{TCE/+}$:R26eYFP* mice were treated with 4OHT and WBI (10 Gy). At 7 dpi, cryosectioned small intestine samples were analyzed for YFP expression.
(K) Comparative analysis of Tert$^+$ and Lgr5$^+$ cell populations after WBI (10 Gy). FACS analysis of Tert$^+$ cells (tdTomato) from *Tert$^{TCE/+}$* and Lgr5$^+$ cells (GFP) from *Lgr5$^{EGFP\text{-}IRES\text{-}creERT2}$* mouse models.
(L) Expression of *Lgr5* in Tert$^+$ cells. *Tert$^{TCE/+}$* mice were treated with WBI (10 Gy; 0, 1, 2 dpi) and subjected to Tert$^+$ cell isolation from intestinal crypts using FACS and qRT-PCR for *Lgr5* expression.
(M) Lineage-tracing of Tert$^+$ cells. *Tert$^{TCE/+}$:R26eYFP* mice were treated with 4OHT and WBI (10 Gy). At 7 dpi, YFP$^+$ cells (arrowhead) were found at the bottom of the crypt between Paneth cells (lysozyme$^+$ cells).
(N–P) Sequential injury-induced Tert$^+$ cell activation. Illustration of Tert$^+$ cell activation by consecutive tissue injuries (N). Scheme of mouse treatment (O). Of note, instead of a lethal dose (10 Gy), a sub-lethal dose WBI (6 Gy) was used, with IdU and CldU. Tert$^+$:IdU$^+$:CldU$^+$ cells were visualized (28 dpi; arrowhead) (P).
The representative images are shown; N ≥ 3; error bars indicate SEM; ns, non-significant ($p \geq 0.05$).

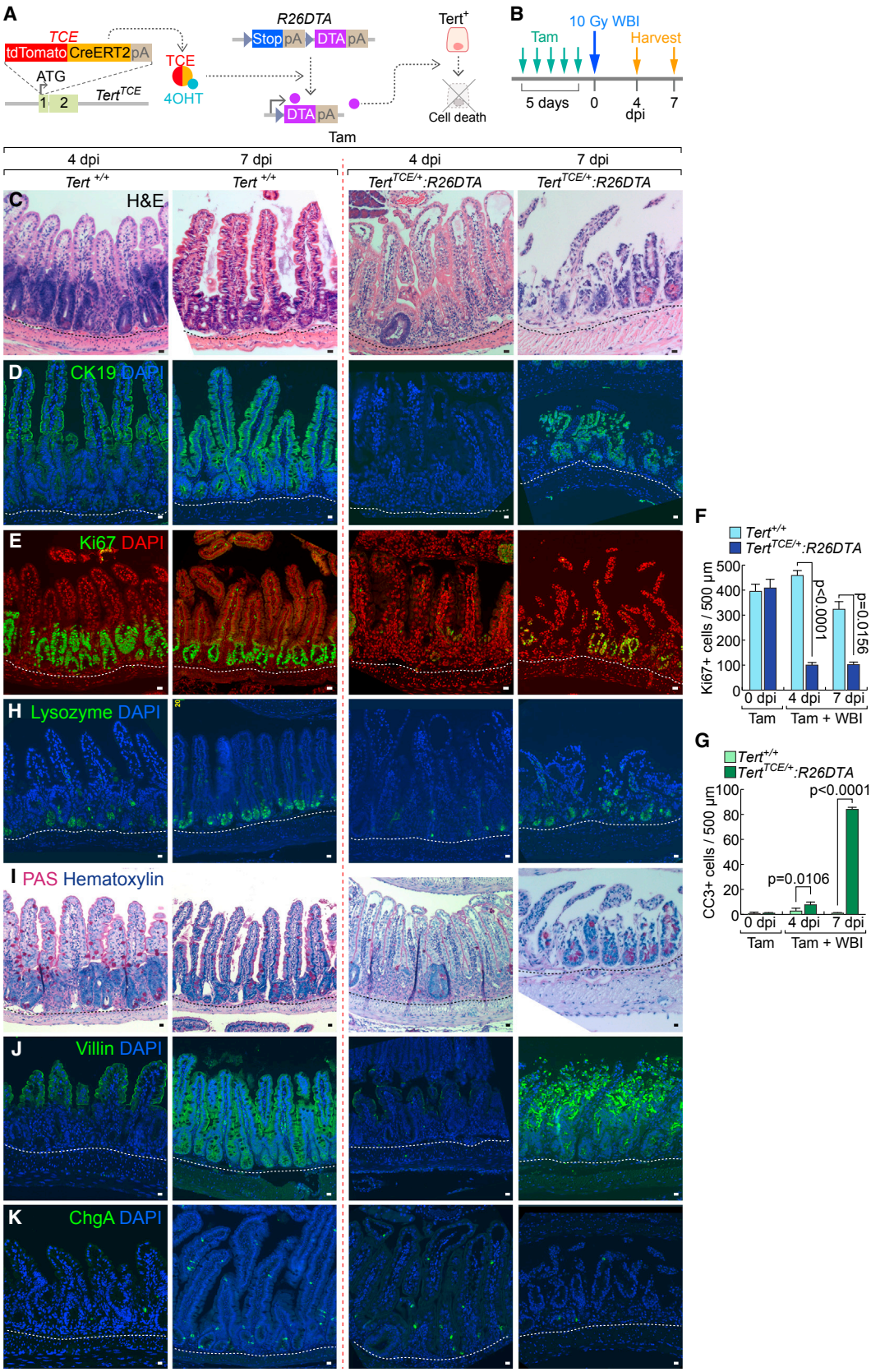

(legend on next page)

Next, we asked how IR upregulates *Wnt2b* in IECs. Given that IR increases reactive oxygen species (ROS) (Azzam et al., 2012) and subsequently activates hypoxia-inducible factors (HIFs) (Moeller et al., 2004), we tested whether the ROS-HIFs signaling axis mediates IR-induced Wnt2b upregulation. Indeed, IR increased ROS generation in the crypt and the normal IECs, represented by the increase of 8-Oxo-2′-deoxyguanosine (8-oxo-dG; an indirect marker of ROS) and 2′,7′-dichlorodihydrofluorescein diacetate (H_2DCFDA; a direct marker of intracellular ROS), respectively (Figures 4J and 4K). Moreover, IR induced the nuclear translocation of HIF1α in the crypt IECs and CCD841CoN IECs (Figures 4L and 4M). Next, we determined whether IR activates HIFs through ROS. We found that the ROS inhibitor, N-acetyl cysteine (NAC), blocked the nuclear translocation of HIF1α in IR-treated CCD841CoN IECs (Figure 4L). Of note, IR also induced the nuclear translocation of HIF2α (Figure S5L). These data suggest that IR-induced HIF activation is mediated by ROS. Furthermore, we found that IR-induced *Wnt2b* upregulation was inhibited by NAC or chetomin (Chet, an inhibitor for HIFs) (Figure 4N), suggesting the potential involvement of ROS and HIFs in IR-induced *Wnt2b* upregulation.

Next, we tested whether HIFs directly transactivate *Wnt2b*. We identified multiple consensus hypoxia response elements (HRE; acgtg) in the conserved noncoding sequences (CNS) of both human and mouse *Wnt2b* promoter (Figure 4O), whereas other Wnt ligands (*Wnt4*, *Wnt5a*, *Wnt6*, *Wnt7b*, and *Wn9a*) harbor fewer HREs (Figure S5J). These results imply that HIFs-transactivated *Wnt2b* might be evolutionarily conserved in mammals. Chromatin immunoprecipitation (ChIP) promoter scanning assays showed that HIF1α conditionally occupied HREs at the *Wnt2b* promoter in mouse small intestine upon IR (Figure 4P). These results suggest that IR induces transactivation of *Wnt2b via* ROS-HIFs (Figure 4Q). Next, we tested whether IR-transactivated *Wnt2b* induces Wnt/β-catenin signaling activation in IECs. In CCD841CoN IECs, treatment of either NAC or Chet suppressed IR-induced upregulation of *Axin2*, a β-catenin target gene (Figure 4R). We also found that ectopic Wnt2b expression is sufficient to activate Wnt/β-catenin signaling, as represented by *Axin2* upregulation in CCD841CoN IECs (Figure 4S). Conversely, depletion of endogenous Wnt2b decreased IR-induced *Axin2* upregulation (Figures 4T and S5C). These data suggest that IR activates Wnt/β-catenin signaling in IECs via the ROS-HIFs-*Wnt2b* signaling axis. Interestingly, it is noteworthy that IR-transactivated *Wnt2b* was only detected in Tert$^-$ IECs, but not in Tert$^+$ cells, in the crypts (Figure 4U). Nonetheless, we found that IR upregulated *Axin2* in Tert$^+$ cells (Figure 4V). To provide clearer evidence that Wnt2b is a critical downstream mediator of regeneration, we also performed knockdown assays for Wnt2b in the single-cell-driven crypt organoids. Using lentivirus encoding short hairpin RNA (shRNA) against *mWnt2b*, we depleted the endogenous Wnt2b and treated the crypt organoids with IR. We found that *Wnt2b* knockdown inhibited the organoid growth under IR-treated conditions (Figures 4W and S5D). It is noteworthy that in the absence of IR treatment, Wnt2b shRNA did not affect the crypt organoid growth. This observation is consistent with the results that *Wnt2b* KO mice are viable without the defects in the intestinal homeostasis (Tsukiyama and Yamaguchi, 2012). These results suggest that IR activates Wnt/β-catenin signaling in Tert$^+$ cells via ROS-HIFs-Wnt2b signaling axis.

Impaired Intestinal Regeneration by β-Catenin Conditional Knockout in Tert$^+$ Cells

Given the requirement of Tert$^+$ cells for intestinal regeneration (Figure 3) and IR-induced activation of Wnt/β-catenin signaling in Tert$^+$ cells (Figure 4V), we hypothesized that IR-activated Wnt/β-catenin signaling contributes to Tert$^+$ ISC activation and subsequent Tert$^+$ cell-driven intestinal regeneration. To test this, we genetically ablated β-catenin/*Ctnnb1* in Tert$^+$ cells by Tam administration into *Tert$^{TCE/+}$: Ctnnb1$^{fl/fl}$* mice (Figures 5A and 5B). Isolated Tert$^+$ cells from the Tam-treated *Tert$^{TCE/+}$: Ctnnb1$^{Δ/Δ}$* strain displayed downregulation of β-catenin target genes (Figure 5C), indicating successful conditional knockout (CKO) of β-catenin/*Ctnnb1*. Next, we examined the effects of β-catenin CKO in Tert$^+$ cells on intestinal regeneration. Indeed, Tam and IR-treated *Tert$^{TCE/+}$: Ctnnb1$^{Δ/Δ}$* mice showed impaired intestinal regeneration, represented by the loss of epithelium integrity, decreased proliferation, increased apoptosis, and abnormal distribution of IEC lineages (Figures 5D–5K). These results suggest that activation of Wnt/β-catenin in Tert$^+$ cells is crucial for intestinal regeneration.

Next, we questioned how Wnt/β-catenin engages in Tert$^+$ cell-mediated intestinal regeneration. Given IR-induced upregulation of cell proliferation-related and β-catenin target genes (*Ccnd1*, *c-Myc, Lgr5, and Axin2*) in Tert$^+$ cells (Figures 2I, 2L, and 4V), we tested whether IR-induced Wnt/β-catenin activation is required for the quiescence exit of Tert$^+$ cells during intestinal regeneration. First, we assessed the effects of β-catenin CKO on the number of the intestinal Tert$^+$ cells. After β-catenin CKO, the number of Tert$^+$ cells was similar between *Tert$^{TCE/+}$* and *Tert$^{TCE/+}$:Ctnnb1$^{Δ/Δ}$* in the homeostatic intestine (no IR) (Figures 5N and S6A). However, FACS analysis showed that β-catenin CKO in Tert$^+$ cells followed by IR reduced the number of proliferative Tert$^+$ cells (Tert$^+$:Ki67$^+$) (Figures 5O and S6B). Moreover, *Ccnd1* and *c-Myc* transcripts were significantly decreased in the small intestine of *Tert$^{TCE/+}$:Ctnnb1$^{Δ/Δ}$* mice upon IR, compared with those in *Tert$^{+/+}$:Ctnnb1$^{+/+}$* mice (Figures 5L and

Figure 3. Impaired Intestinal Regeneration by Conditional Ablation of Tert$^+$ Cells

(A) Illustration of conditional ablation of Tert$^+$ cells (*Tert$^{TCE/+}$:R26DTA*). 4OHT treatment activates TCE, which leads to the expression of diphtheria toxin A (DTA) for Tert$^+$ cell ablation.

(B) Scheme of mouse treatment.

(C–K) Impairment of intestinal regeneration by Tert$^+$ cell ablation. H&E staining (C); cytokeratin 19 (CK19) (D); Ki67 (E); lysozyme (Paneth cell, H; PAS (goblet cell, I; villin (enterocyte, J; chromogranin A (ChgA; enteroendocrine cell, K). Of note, Tam-treated *Tert$^{TCE/+}$:R26DTA* did not affect intestinal homeostasis (Figures S3B–S3I). Quantification of the number of Ki67$^+$ cells (F) and CC3$^+$ cells (G) per 500-μm region of crypts. Scale bars, 20 μm; dot lines indicate the basal membranes below crypts.

The representative images are shown; N ≥ 3.

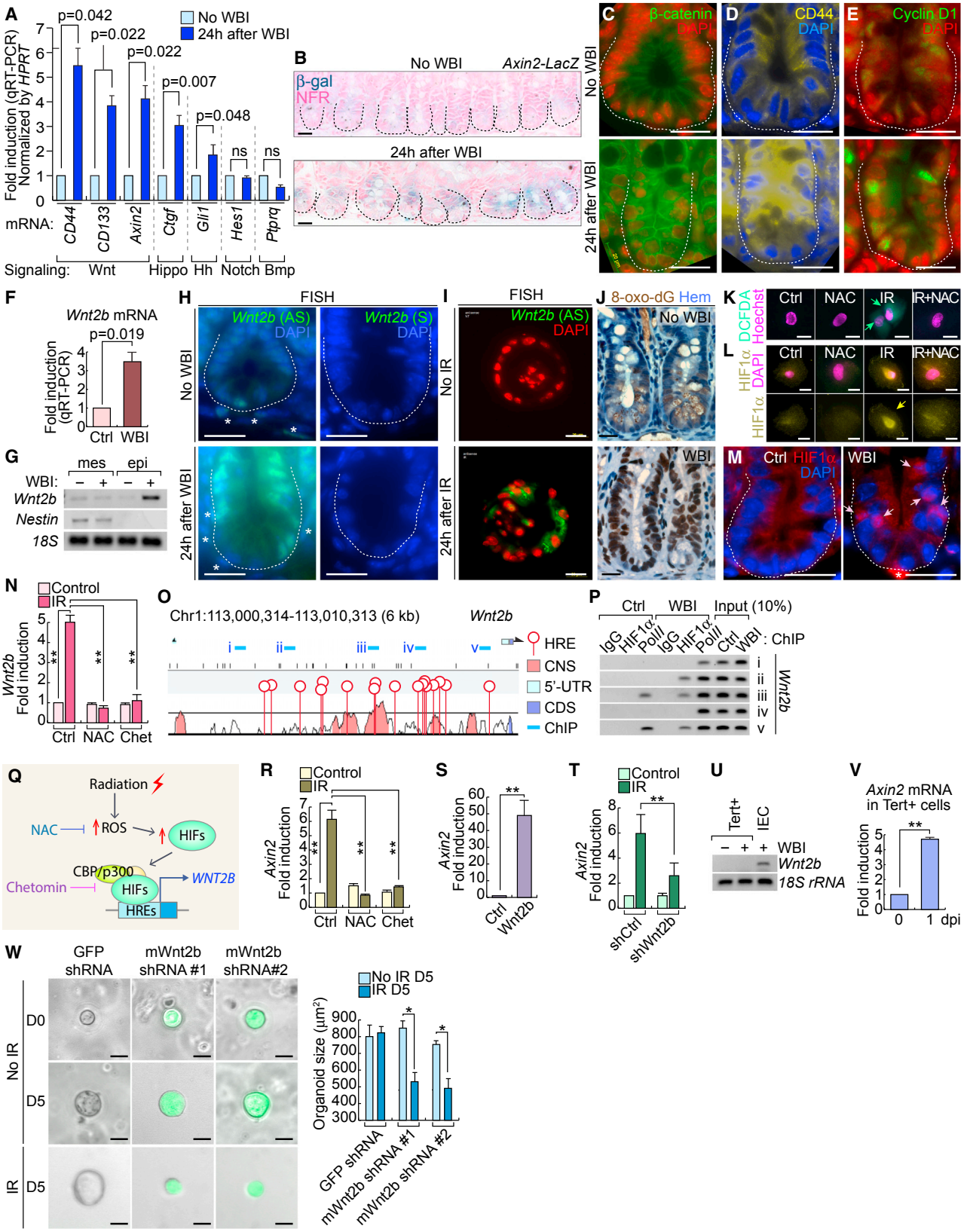

(legend on next page)

5M). These results suggest that IR-activated Wnt/β-catenin signaling is required for the transition of Tert$^+$ cells from quiescent to proliferative status upon tissue injury.

DISCUSSION

The quiescent ISCs have been identified as Bmi1 or *Hopx*-expressing cells as well as BrdU-retaining secretory precursors (Buczacki et al., 2013; Takeda et al., 2011; Sangiorgi and Capecchi, 2008). Interestingly, we observed that not all Tert$^+$ cells were colocalized with Bmi1$^+$ cells (see Figure 1K), indicating Tert$^+$ ISCs are somewhat distinguished from Bmi1$^+$ ISCs. Furthermore, unlike Buczacki's LRCs (Buczacki et al., 2013), the markers of Tert$^+$ LRCs partially overlapped only with enteroendocrine cells, but not Paneth cells (see Figures 1L–1N), which suggest the existence of additional quiescent ISCs. Although we here limited our scope to Tert$^+$ LRCs, it is probable that the different ISCs coordinately serve as multiple sources for repopulation into IECs during intestinal regeneration.

Importantly, given the contrasting kinetics of Lgr5$^+$ and Tert$^+$ cell populations (see Figure 2K), the marked induction of *Lgr5* expression in Tert$^+$ cells (see Figure 2L), and Tert$^+$ cell-driven progeny at the bottom of the crypt during regeneration (see Figure 2M), it is highly conceivable that the acute loss of Lgr5$^+$ cells by IR might be compensated by Tert$^+$ cells. Similarly, Hopx$^+$ and Bmi1$^+$ cells give rise to Lgr5$^+$ cells *ex vivo* (Takeda et al., 2011; Tian et al., 2011). This is consistent with the results that neither genetic ablation nor IR-induced removal of Lgr5$^+$ ISCs impairs intestinal integrity (Yan et al., 2012; Tian et al., 2011). Therefore, it is highly likely that despite the removal of Lgr5$^+$ cells, Tert$^+$ cells serve as a reservoir for Lgr5$^+$ cells during regeneration. This is also supported by our results that the ablation of Tert$^+$ cells severely impairs intestinal regeneration (see Figures 3C–3K). Intriguingly, despite the crucial roles of Tert$^+$ cells in intestinal regeneration, the removal of Tert$^+$ cells did not affect intestinal homeostasis (see Figures S3C–S3J). Considering the cell plasticity in various regenerative tissue such as pancreas (Kopp et al., 2016), intestine (Tetteh et al., 2016; Asfaha et al., 2015; van Es et al., 2012), and lung (Tata et al., 2013), our working model does not fully exclude the possibility that Tert$^+$ cells are generated from Tert$^-$ cells during intestinal regeneration, which should be carefully examined using the compound lineage-tracing experiments. Nonetheless, during intestinal homeostasis, no Tert$^+$ cells were generated (up to 30 days) after Tert$^+$ cell ablation (see Figures S4A and S4B), implying no *de novo* development of Tert$^+$ cells, at least, during intestinal homeostasis.

Employing our knockin mouse model, we elucidate that Wnt/β-catenin signaling is required for the transition of Tert$^+$ cells from quiescence to mitotic activation. We observed that IR creates multiple DNA damage foci in most IECs in the crypts (see Figure 2B). IR directly induces DNA damage by random DNA breaks or indirectly through reactive oxygen species (ROS) generated by water hydrolysis (Azzam et al., 2012). Although excessive ROS induces cell death, a moderate increase of ROS can regulate the activity of several downstream proteins

Figure 4. IR-Activated Wnt/β-Catenin Signaling in the Crypts and Tert$^+$ Cells

(A) IR-induced upregulation of Wnt signaling target genes (*CD44*, *CD133*, and *Axin2*). qRT-PCR of intestinal crypts isolated from mice treated with WBI (10 Gy, 24 hpi).

(B–E) IR-induced Wnt/β-catenin signaling activation in intestinal crypt. WBI (10 Gy, 24 hpi). X-gal staining in *Axin2-LacZ* intestine (B) and IHC for β-catenin (C), CD44 (D), and Cyclin D1 (E). Scale bars, 20 μm.

(F) *Wnt2b* upregulation in crypts by WBI (10 Gy, 24 hpi). qRT-PCR.

(G) IR-induced *Wnt2* upregulation in the crypt epithelial cells. WBI (10 Gy, 24 hpi). Semiquantitative (sq) RT-PCR.

(H) *Wnt2* upregulation in crypts by WBI (10 Gy). Fluorescence *in situ* hybridization (FISH). AS, antisense; S, sense probes. Scale bars, 20 μm. An asterisk indicates Wnt2b$^+$ mesenchymal cells.

(I) *Wnt2* upregulation in crypt organoids by IR (8 Gy). Fluorescence *in situ* hybridization (FISH). AS, antisense. Scale bars, 20 μm.

(J) IR-induced ROS generation in the crypt. IHC for 8-Oxo-2′-deoxyguanosine (8-oxo-dG). Scale bars, 20 μm.

(K) IR-induced ROS generation in CCD841CoN IEC cells (10 Gy, 0.5 hr). DCFDA staining.

(L) IR-induced HIF1α activation via ROS in CCD841CoN. Cells were pre-treated with N-acetyl-L-cysteine (NAC, 1 mM) for 4 hr and exposed to IR (10 Gy). After 24 hr, cells were analyzed by IF staining for HIF1α. Scale bars, 20 μm.

(M) IR-induced HIF1α nuclear translocation in the crypt. WBI (10 Gy, 24 hpi); scale bars, 20 μm. An asterisk indicates non-specific signal.

(N) IR-induced *Wnt2* transactivation via ROS-HIFs in CCD841CoN. Cells were pre-treated with NAC or chetomin (100 nM) for 4 hr. After IR exposure (10 Gy, 24 hr), cells were analyzed for qRT-PCR.

(O) *Wnt2b* promoter analysis for hypoxia response element (HRE). Conserved non-coding sequence (CNS); coding sequence (CDS); and 5 ChIP amplicons (i–v).

(P) IR-induced recruitment of HIF1α to *Wnt2b* promoter in the small intestine. Small intestine samples from mice (±WBI [10 Gy], 24 hr) were analyzed for ChIP assays. RNA polymerase II (Pol II) served as a positive control for transcriptional activation.

(Q) Illustration of radiation-induced Wnt/β-catenin signaling activation via ROS-HIFs-Wnt2b.

(R) Inhibition of IR-induced *Axin2* by NAC or chetomin. CCD841CoN cells were pre-treated with NAC or chetomin, treated with IR (10 Gy, 24 hr), and analyzed by qRT-PCR.

(S) Wnt2b-activated β-catenin signaling activation. CCD841CoN cells were transfected with *Wnt2b* expression plasmids. 24 hr after transfection, cells were analyzed by qRT-PCR for *Axin2*.

(T) Wnt2b mediates IR-induced Wnt/β-catenin signaling activation. CCD841CoN cells were stably transduced with lentiviruses encoding shRNAs against *Wnt2b* and then treated with IR (10 Gy, 24 hr), followed by qRT-PCR analysis of *Axin2*.

(U) No expression of *Wnt2b* in Tert$^+$ cells. Semiquantitative (sq) RT-PCR. IECs isolated from the crypts served as positive control.

(V) *Axin2* upregulation by IR in Tert$^+$ cells. qRT-PCR of *Axin2* in Tert$^+$ cells isolated from *Tert$^{TCE/+}$* mice treated with WBI (10 Gy; 1 dpi).The representative images are shown; N ≥ 3; error bars indicate SEM. **p < 0.05.

(W) Knockdown of *Wnt2b* in crypt single-cell organoids. Lentiviruses expressing mouse *Wnt2b* shRNAs (clone #1∼#2) inhibited organoid growth after IR (4 Gy). GFP shRNA was used as a negative control. Scale bars, 20 μm; *p < 0.05.

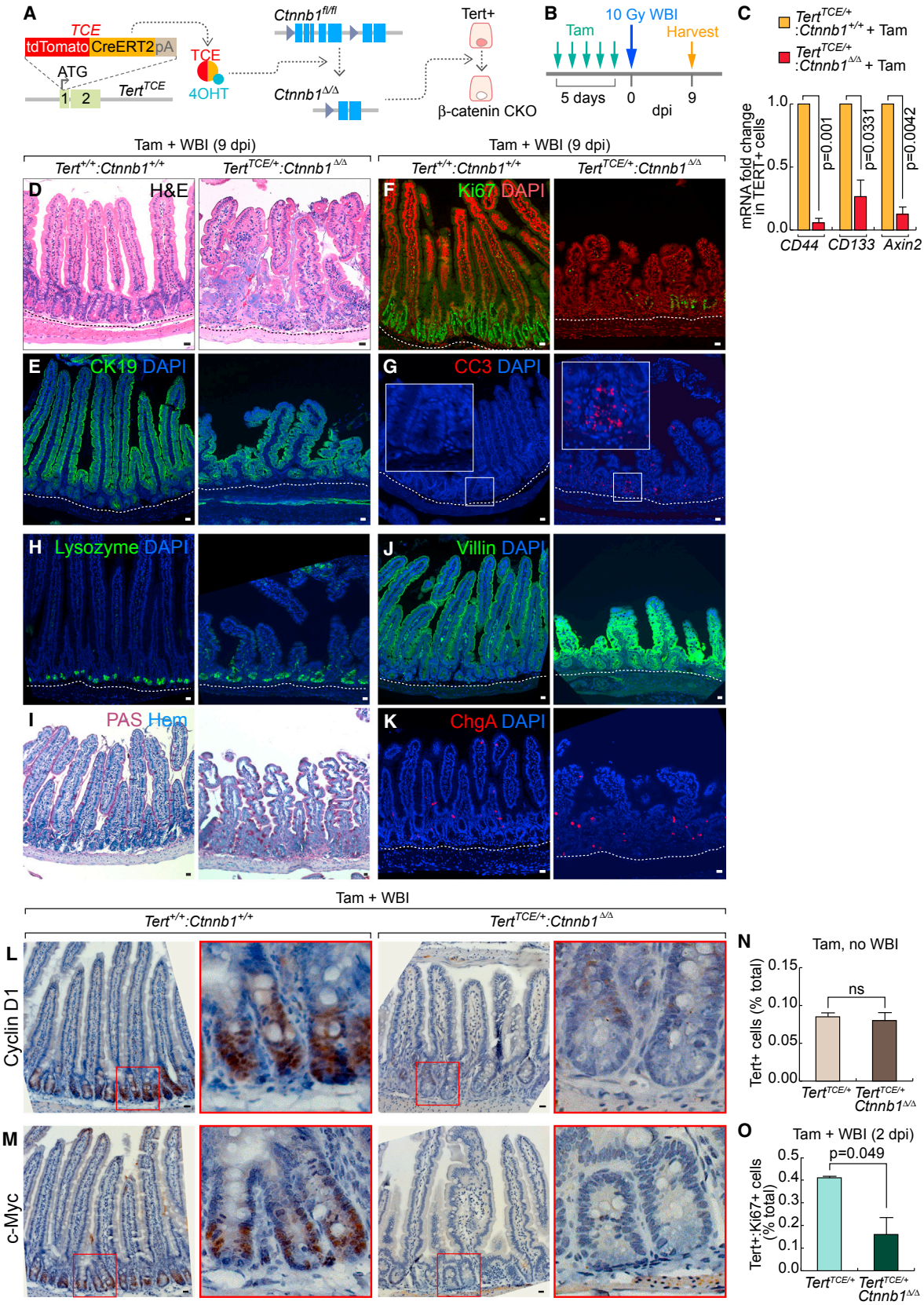

(legend on next page)

including HIFs (Niecknig et al., 2012; Gerald et al., 2004). Indeed, IR increased ROS in the intestine followed by the direct recruitment of HIF-1α to the *Wnt2b* promoter and subsequent *Wnt2b* transactivation (see Figures 4J and 4P). Furthermore, given the inhibitory effects of Chet on both HIF-1α and HIF-2α and the protective role of HIF-2α in the intestine (Taniguchi et al., 2014; Xie et al., 2014), HIF-2α might also be involved in ROS-mediated *Wnt2b* transactivation.

We recently found that IR acutely activates Wnt/β-catenin signaling and transactivates *LIG4*, a core component of non-homologous end joining repair (Jun et al., 2016). However, the detailed molecular mechanism of IR-activated Wnt/β-catenin signaling remained elusive. Our unbiased screening results of signaling pathways and Wnt ligands led us to select Wnt2b and the Wnt/β-catenin pathway as important mediators of Tert$^+$ cell activation during intestinal regeneration. Wnt2b functionally compensates for the loss of epithelial Wnt3 in crypt organoid culture (Farin et al., 2012; Goss et al., 2009), indicating a role of Wnt2b in transducing canonical Wnt signaling. We found that IR markedly upregulates *Wnt2b* in IECs near +4, but not in Tert$^+$, cells (see Figures 4H and 4U), and *Wnt2b* knockdown inhibited organoid growth upon IR (see Figure 4W). Of note, Wnt2b was shown to activate canonical Wnt signaling (β-catenin-mediated) (Goss et al., 2009). We found that IR activates Wnt/β-catenin signaling in Tert$^+$ cells (see Figure 4V), suggesting that IR-induced Wnt2b in IECs activates Wnt signaling in Tert$^+$ cells. Moreover, the results from β-catenin CKO in Tert$^+$ cells clearly demonstrated the requirement of Wnt/β-catenin signaling in Tert$^+$ cell activation and Tert$^+$ cell-driven intestinal regeneration (see Figures 5D–5K). Wnt signaling plays multiple roles in SC regulation including SC maintenance, activation, and differentiation (Lien and Fuchs, 2014). In our experimental condition, we found that β-catenin CKO in Tert$^+$ cells did not affect the number of Tert$^+$ cells but instead, suppressed the quiescence exit of Tert$^+$ cells (see Figures 5N and 5O). This is also consistent with the reduced expression of cell proliferation-related genes in β-catenin CKO in Tert$^+$ cells (see Figures 5L and 5M). Thus, our results strongly suggest that β-catenin is essential for the quiescence exit of Tert$^+$ cells during intestinal regeneration.

Despite the significance of Tert as a catalytic subunit of telomerase in self-renewing cells, the absence of accurate Tert reporter mouse models made it difficult to study Tert$^+$ cells. Unlike previous transgenic mice generated by pronuclear injection of *Tert* promoter-CreER DNA (Montgomery et al., 2011), our model is a knockin mouse strain established by blastocyst injection of targeted mouse embryonic stem cells. Given the limitation of transgenic mice mainly due to the random integration and uncontrolled copy number of the foreign DNA, gene targeting (knockin) is more specific and reliable for representing physiological and pathological events of Tert$^+$ cells. Moreover, our *Tert* knockin mouse model not only visualizes Tert$^+$ cells with tdTomato fluorescence, but also enables us to perform various cellular and genetic manipulation of Tert$^+$ cells using a CreERT2 cassette. Given that Tert is expressed in the self-renewing cells, future studies employing *Tert*$^{TCE/+}$ mice in different tissue (pancreas, liver, kidney, and hair follicle) may provide valuable insights into our understanding of tissue SCs. Furthermore, due to the reactivation of telomerase in human cancer, our *Tert* mouse models can also be used to isolate and characterize self-renewing tumor cells.

Together, our results define Tert$^+$ cells as essential ISCs for tissue regeneration and unveil how Tert$^+$ ISCs are conditionally activated from the quiescent state upon tissue injury (see Figure 6).

EXPERIMENTAL PROCEDURES

Animals

All mice were maintained in compliance with the Institutional Animal Care and Use Committee's (IACUC) guidelines at the MD Anderson Cancer Center. Male and female mice (older than 6 weeks) were used for experiments. *Gt(ROSA)26Sor*$^{tm1(EYFP)Cos}$/J (Jax strain 006148), *Gt(ROSA)26Sor*$^{tm1(DTA)Lky}$/J (Jax strain 009669), *Ctnnb1*^{tm2Kem}/*KnwJ* (Jax strain 004152), and *Axin2*^{LacZ} (Jax strain 009120) were purchased from Jackson Laboratory. Genotyping was performed following the Jackson Laboratory's protocol. Tam was dissolved in corn oil (Fisher) at a final concentration of 10 mg/mL for intraperitoneal (i.p.) administration (50 mg/kg). For intestine injury, mice were exposed to 10 or 6 Gy (non-lethal dose for cell labeling) WBI, and tissue was collected at multiple time points.

Label-Retaining Cell Assay

Tert$^{TCE/+}$ mice were intraperitoneally administrated with BrdU (Sigma) (1 mg) at age 2 weeks. The tissue sample was collected at age 12 weeks and analyzed for Tert$^+$:BrdU$^+$ cells in the crypt.

FACS Analysis

Intestinal crypts were isolated from *Tert*$^{TCE/+}$ mice. For single-cell isolation, crypts were digested with Accumax (Stem Cell Technology 07921) for 20 min and collected through 70- (BD 087712) and 40-μm (BD 087711) cell strainers. Next, cells were suspended in PBS with 10% fetal bovine serum (FBS) and stained with SYTOX Blue (Life Technologies S34857) to exclude

Figure 5. Impaired Intestinal Regeneration by β-Catenin Conditional Knockout in Tert$^+$ Cells

(A) Illustration of β-catenin/*Ctnnb1* conditional knockout (CKO) in Tert$^+$ cells (*TERT*$^{TCE/+}$;*Ctnnb1*$^{fl/fl}$).

(B) Scheme of mouse treatment.

(C) β-catenin CKO-induced downregulation of Wnt/β-catenin target gene expression in Tert$^+$ cells. qRT-PCR of Tert$^+$ cells for *CD44, CD133*, and *Axin2* expression from *Tert*$^{TCE/+}$ (control) and *Tert*$^{TCE/+}$:*Ctnnb1*$^{\Delta/\Delta}$ (experimental group) treated with tamoxifen.

(D–K) IHC of impaired intestinal regeneration by β-catenin CKO in Tert$^+$ cells. H&E staining (D); CK19 (E); Ki67 (F); CC3 (G); lysozyme (H); PAS (I); villin (J); and ChgA (K). Scale bars, 20 μm.

(L and M) Cell cycle-related gene expression in *Tert*$^{+/+}$;*Ctnnb1*$^{+/+}$ and *Tert*$^{TCE/+}$;*Ctnnb1*$^{\Delta/\Delta}$ (10 Gy, 7 dpi). Cyclin D1 (L) and c-Myc (M) were significantly downregulated by β-catenin CKO in Tert$^+$ cells and WBI. Scale bars, 20 μm.

(N) No loss of Tert$^+$ cells by β-catenin CKO during intestinal homeostasis. Population analysis of Tert$^+$ cells after Tam treatment in *Tert*$^{TCE/+}$ and *Tert*$^{TCE/+}$;*Ctnnb1*$^{\Delta/\Delta}$, using FACS. ns: non-significant ($p > 0.05$).

(O) Reduced proliferation of Tert$^+$ cells during intestinal regeneration by β-catenin CKO. Quantification of Tert$^+$:Ki67$^+$ cells of Tam and IR (10 Gy; 2 dpi)-treated *Tert*$^{TCE/+}$ and *Tert*$^{TCE/+}$;*Ctnnb1*$^{\Delta/\Delta}$ mice, using FACS.

The representative images are shown; N ≥ 3; error bars indicate SEM.

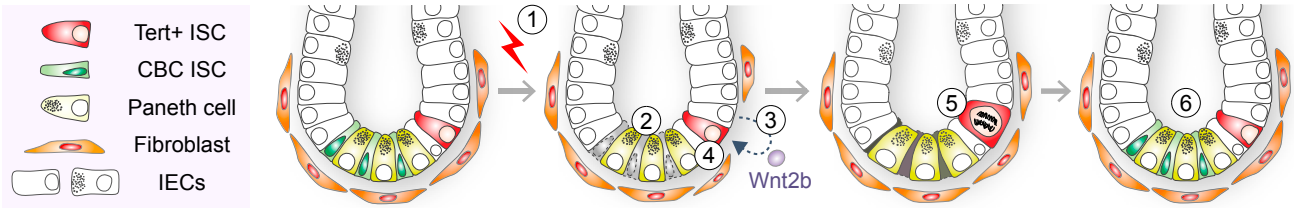

Figure 6. Illustration of Working Model

IR induces the death of mitotic cells (TA and CBC ISCs) in the crypts. (1–2) Simultaneously, IR transactivates *Wnt2b via* ROS-HIFs in IECs (3) and activates Wnt/β-catenin signaling in Tert$^+$ cells (4), which results in the quiescence exit of Tert$^+$ cells (5). Repopulation of Tert$^+$ cells generates the progenitor and differentiated IECs (6). Finally, Tert$^+$ cells re-enter into the quiescent state.

dead cells. tdTomato fluorescence was detected by FACS (MoFlo Astrios, Beckman Coulter) and sorted into Tert$^+$ and Tert$^-$ cells among live cells based on the gate. Sorted Tert$^+$ and Tert$^-$ cells were analyzed for single-cell gene expression profiling. To quantify the proliferation of Tert$^+$ cells, single cells isolated from crypt were fixed with 4% paraformaldehyde, blocked, incubated with a fluorescein isothiocyanate (FITC)-conjugated Ki67 antibody, and stained with DAPI. The population of Tert$^+$:Ki67$^+$ was assessed by FACS (Gallios 561, Beckman Coulter).

Gene Expression Analysis

Isolated Tert$^+$ and Tert$^-$ cells ($\lesssim$5 cells) were synthesized to complementary DNA (cDNA) using a REPLI-g WTA Single Cell Kit (QIAGEN) and analyzed for single-cell gene expression. For gene expression analysis, isolated crypts were processed for RNA extraction (QIAGEN RNeasy Mini Kit) and RT (iScript RT Supermix for qRT-PCR, Biorad). 18S ribosomal RNA (*18S rRNA*) was used as an endogenous control for normalization. qRT-PCR was performed using intron-spanning primers. Fold induction was quantified using the $2^{-\Delta\Delta CT}$ method. For Figure 1J, ΔΔCT values were displayed using heatmap software (http://bar.utoronto.ca/). Primer sequences are listed in Table S1.

Dual-Pulse Labeling Assay

Tert$^{TCE/+}$ mice were treated for the first tissue injury (6 Gy WBI) followed by 5-iodo-2′-deoxyuridine (IdU, Sigma) (1 mg) i.p. injection. 2 weeks later, Tert$^{TCE/+}$ mice were treated for the second tissue injury (6 Gy WBI), followed by 5-chloro-2′-deoxyuridine (CldU, Sigma) (1 mg) i.p. injection. After 2 weeks, the tissue was collected and analyzed for Tert$^+$:IdU$^+$:CldU$^+$ cells in the crypts.

FISH

FISH was performed in accordance with the manufacturer's protocol (Invitrogen, FISH Tag RNA Green Kit, with Alexa Fluor 488 dye). Complementary probes were designed for the coding sequences *Wnt2b* (441 bp), *Wnt4* (421 bp), *Wnt5a* (437 bp), *Wnt6* (476 bp), *Wnt7b* (570 bp), and *Wnt9a* (401 bp). PCR products of Wnt ligands were inserted and transformed using TOPO-TA Cloning (Invitrogen). Linearized plasmids (sense and antisense) were subjected to transcription, purification (anime-modified RNA), and labeling with the fluorescent dye (Alexa Fluor 488). Intestine tissue slides were deparaffinized, processed for antigen retrieval (proteinase K, 10 μg/mL), and incubated with hybridization buffer (50% formamide, 5× saline sodium citrate [SSC], 100 μg/mL fragmented salmon testes DNA, 50 μg/mL heparin, and 0.1% Tween20). Tissue slides were then incubated with probe-fluorescent dye in hybridization buffer (1 μg/mL) at 55°C in a water bath for 20 hr. The next day, slides were washed with hybridization buffer, 50% hybridization buffer/PBS with 0.1% Tween 20 (PBT), and PBT. Slides were soaked with 70% glycerol/30% PBT, counterstained with 30 nM DAPI (Molecular Probes), and mounted with SlowFade Gold Antifade Mountant (Thermo). A sense probe was used as a negative control.

In Silico Promoter Analysis

Conserved noncoding sequences (CNSs) were analyzed using the VISTA genome browser (http://genome.lbl.gov/vista). Briefly, the human and the mouse *Wnt* ligands promoters were analyzed with default options (200-bp window, x axis; 70% conservancy, y axis) for potential hypoxia response elements (HREs; balloons). Promoter regions where peak values (y axis) are above 50% were considered as potent evolutionarily conserved regulated elements.

ChIP Assays

Mouse intestine (non-treated and IR) was minced into small pieces, cross-linked with 1% formaldehyde for 15 min at room temperature (RT), and quenched by glycine (0.125 M). After washing with cold PBS, tissue was incubated with lysis buffer (0.5% NP-40, 25 mM HEPES, 150 mM KCl, 1.5 mM MgCl2, 10% glycerol, and KOH [pH 7.5]) containing protease inhibitor for 15 min on ice. Cell lysates were centrifuged (5,000 rpm for 5 min), and supernatants were discarded. Cell pellets were then subjected to sonication with a ChIP-radioimmunoprecipitation assay (RIPA) lysis buffer (50 mM Tris [pH 8.0], 150 mM NaCl, 0.1% SDS, 0.5% deoxycholate, 1% NP-40, and 1 mM EDTA; 10 times, 30 s on/30 s off), using a Bioruptor Plus sonication device (Diagnode, NJ, USA). After centrifugation (13,200 rpm for 30 min), a supernatant was immunoprecipitated with antibody overnight at 4°C and was pulled down using Dynabeads Magnetic Beads (Thermo). Immunoprecipitates were further washed serially with a ChIP-RIPA lysis buffer, high-salt buffer (50 mM Tris [pH 8.0], 500 mM NaCl, 0.1% SDS, 0.5% deoxycholate, 1% NP-40, and 1 mM EDTA), LiCl wash buffer (50 mM Tris [pH 8.0], 1 mM EDTA, 250 mM LiCl, 1% NP-40, and 0.5% deoxycholate), and Tris-EDTA buffer. Finally, immunoprecipitate crosslinking was reversed by incubation at 65°C overnight and treated with RNase A and proteinase K to extract DNA. ChIP amplicons (i–v) were detected via ChIP-PCR. Primer sequences for ChIP-PCR are available in Table S1.

Statistical Analyses

The Student's t test was used for comparisons of two samples. p values < 0.05 were considered significant. Error bars indicate SEM. The number of biological and experimental replicates is ≥ 3, unless otherwise mentioned in the figure legends.

SUPPLEMENTAL INFORMATION

Supplemental Information includes Supplemental Experimental Procedures, six figures, and two tables and can be found with this article online at https://doi.org/10.1016/j.celrep.2017.10.118.

AUTHOR CONTRIBUTIONS

H.N.S. and J.-I.P. conceived the experiments. H.N.S., M.J.K., Y.-S.J., E.M.L., S.J., and J.-I.P. performed the experiments. H.N.S. and J.-I.P. analyzed the data. H.N.S. and J.-I.P. wrote the manuscript.

ACKNOWLEDGMENTS

We thank Pierre D. McCrea, Junjie Chen, Seung-Hyo Lee, and Christopher L. Cervantes for helpful comments on the manuscript. This work was supported by the Cancer Prevention and Research Institute of Texas (RP140563), the NIH (CA193297-01, CA098258), the Department of Defense (CA140572), a Duncan Family Institute for Cancer Prevention and Risk Assessment grant

(IRG-08-061-01), a Center for Stem Cell and Developmental Biology Transformative grant (MD Anderson Cancer Center), an Institutional Research grant (MD Anderson Cancer Center), a New Faculty Award (CA016672), and a Metastasis Research Center grant (MD Anderson Cancer Center). The Genetically Engineered Mouse Facility was supported by an MD Anderson Cancer Center support grant (CA016672).

Received: June 12, 2017
Revised: October 3, 2017
Accepted: October 29, 2017
Published: November 28, 2017

REFERENCES

Asfaha, S., Hayakawa, Y., Muley, A., Stokes, S., Graham, T.A., Ericksen, R.E., Westphalen, C.B., von Burstin, J., Mastracci, T.L., Worthley, D.L., et al. (2015). Krt19(+)/Lgr5(-) cells are radioresistant cancer-initiating stem cells in the colon and intestine. Cell Stem Cell *16*, 627–638.

Azzam, E.I., Jay-Gerin, J.P., and Pain, D. (2012). Ionizing radiation-induced metabolic oxidative stress and prolonged cell injury. Cancer Lett. *327*, 48–60.

Barker, N. (2014). Adult intestinal stem cells: critical drivers of epithelial homeostasis and regeneration. Nat. Rev. Mol. Cell Biol. *15*, 19–33.

Bhanja, P., Saha, S., Kabarriti, R., Liu, L., Roy-Chowdhury, N., Roy-Chowdhury, J., Sellers, R.S., Alfieri, A.A., and Guha, C. (2009). Protective role of R-spondin1, an intestinal stem cell growth factor, against radiation-induced gastrointestinal syndrome in mice. PLoS ONE *4*, e8014.

Blanpain, C., Lowry, W.E., Pasolli, H.A., and Fuchs, E. (2006). Canonical notch signaling functions as a commitment switch in the epidermal lineage. Genes Dev. *20*, 3022–3035.

Buczacki, S.J., Zecchini, H.I., Nicholson, A.M., Russell, R., Vermeulen, L., Kemp, R., and Winton, D.J. (2013). Intestinal label-retaining cells are secretory precursors expressing Lgr5. Nature *495*, 65–69.

Choi, Y.S., Zhang, Y., Xu, M., Yang, Y., Ito, M., Peng, T., Cui, Z., Nagy, A., Hadjantonakis, A.K., Lang, R.A., et al. (2013). Distinct functions for Wnt/β-catenin in hair follicle stem cell proliferation and survival and interfollicular epidermal homeostasis. Cell Stem Cell *13*, 720–733.

Eisenhoffer, G.T., Loftus, P.D., Yoshigi, M., Otsuna, H., Chien, C.B., Morcos, P.A., and Rosenblatt, J. (2012). Crowding induces live cell extrusion to maintain homeostatic cell numbers in epithelia. Nature *484*, 546–549.

Farin, H.F., Van Es, J.H., and Clevers, H. (2012). Redundant sources of Wnt regulate intestinal stem cells and promote formation of Paneth cells. Gastroenterology *143*, 1518–1529 e7.

Flores, I., Benetti, R., and Blasco, M.A. (2006). Telomerase regulation and stem cell behaviour. Curr. Opin. Cell Biol. *18*, 254–260.

Gerald, D., Berra, E., Frapart, Y.M., Chan, D.A., Giaccia, A.J., Mansuy, D., Pouysségur, J., Yaniv, M., and Mechta-Grigoriou, F. (2004). JunD reduces tumor angiogenesis by protecting cells from oxidative stress. Cell *118*, 781–794.

Goss, A.M., Tian, Y., Tsukiyama, T., Cohen, E.D., Zhou, D., Lu, M.M., Yamaguchi, T.P., and Morrisey, E.E. (2009). Wnt2/2b and beta-catenin signaling are necessary and sufficient to specify lung progenitors in the foregut. Dev. Cell *17*, 290–298.

Hiyama, E., and Hiyama, K. (2007). Telomere and telomerase in stem cells. Br. J. Cancer *96*, 1020–1024.

Hsu, Y.C., and Fuchs, E. (2012). A family business: stem cell progeny join the niche to regulate homeostasis. Nat. Rev. Mol. Cell Biol. *13*, 103–114.

Itzkovitz, S., Lyubimova, A., Blat, I.C., Maynard, M., van Es, J., Lees, J., Jacks, T., Clevers, H., and van Oudenaarden, A. (2011). Single-molecule transcript counting of stem-cell markers in the mouse intestine. Nat. Cell Biol. *14*, 106–114.

Jun, S., Jung, Y.S., Suh, H.N., Wang, W., Kim, M.J., Oh, Y.S., Lien, E.M., Shen, X., Matsumoto, Y., McCrea, P.D., et al. (2016). LIG4 mediates Wnt signalling-induced radioresistance. Nat. Commun. *7*, 10994.

Kim, K.A., Kakitani, M., Zhao, J., Oshima, T., Tang, T., Binnerts, M., Liu, Y., Boyle, B., Park, E., Emtage, P., et al. (2005). Mitogenic influence of human R-spondin1 on the intestinal epithelium. Science *309*, 1256–1259.

Kopp, J.L., Grompe, M., and Sander, M. (2016). Stem cells versus plasticity in liver and pancreas regeneration. Nat. Cell Biol. *18*, 238–245.

Lien, W.H., and Fuchs, E. (2014). Wnt some lose some: transcriptional governance of stem cells by Wnt/β-catenin signaling. Genes Dev. *28*, 1517–1532.

Lim, X., Tan, S.H., Koh, W.L., Chau, R.M., Yan, K.S., Kuo, C.J., van Amerongen, R., Klein, A.M., and Nusse, R. (2013). Interfollicular epidermal stem cells self-renew via autocrine Wnt signaling. Science *342*, 1226–1230.

Lowell, S., Jones, P., Le Roux, I., Dunne, J., and Watt, F.M. (2000). Stimulation of human epidermal differentiation by delta-notch signalling at the boundaries of stem-cell clusters. Curr. Biol. *10*, 491–500.

Marinari, E., Mehonic, A., Curran, S., Gale, J., Duke, T., and Baum, B. (2012). Live-cell delamination counterbalances epithelial growth to limit tissue overcrowding. Nature *484*, 542–545.

Moeller, B.J., Cao, Y., Li, C.Y., and Dewhirst, M.W. (2004). Radiation activates HIF-1 to regulate vascular radiosensitivity in tumors: role of reoxygenation, free radicals, and stress granules. Cancer Cell *5*, 429–441.

Montgomery, R.K., Carlone, D.L., Richmond, C.A., Farilla, L., Kranendonk, M.E., Henderson, D.E., Baffour-Awuah, N.Y., Ambruzs, D.M., Fogli, L.K., Algra, S., and Breault, D.T. (2011). Mouse telomerase reverse transcriptase (mTert) expression marks slowly cycling intestinal stem cells. Proc. Natl. Acad. Sci. USA *108*, 179–184.

Muñoz, J., Stange, D.E., Schepers, A.G., van de Wetering, M., Koo, B.K., Itzkovitz, S., Volckmann, R., Kung, K.S., Koster, J., Radulescu, S., et al. (2012). The Lgr5 intestinal stem cell signature: robust expression of proposed quiescent '+4' cell markers. EMBO J. *31*, 3079–3091.

Niecknig, H., Tug, S., Reyes, B.D., Kirsch, M., Fandrey, J., and Berchner-Pfannschmidt, U. (2012). Role of reactive oxygen species in the regulation of HIF-1 by prolyl hydroxylase 2 under mild hypoxia. Free Radic. Res. *46*, 705–717.

Potten, C.S., Owen, G., and Booth, D. (2002). Intestinal stem cells protect their genome by selective segregation of template DNA strands. J. Cell Sci. *115*, 2381–2388.

Psarras, S., Karagianni, N., Kellendonk, C., Tronche, F., Cosset, F.L., Stocking, C., Schirrmacher, V., Boehmer Hv, Hv., and Khazaie, K. (2004). Gene transfer and genetic modification of embryonic stem cells by Cre- and Cre-PR-expressing MESV-based retroviral vectors. J. Gene Med. *6*, 32–42.

Saha, S., Bhanja, P., Kabarriti, R., Liu, L., Alfieri, A.A., and Guha, C. (2011). Bone marrow stromal cell transplantation mitigates radiation-induced gastrointestinal syndrome in mice. PLoS ONE *6*, e24072.

Saha, S., Aranda, E., Hayakawa, Y., Bhanja, P., Atay, S., Brodin, N.P., Li, J., Asfaha, S., Liu, L., Tailor, Y., et al. (2016). Macrophage-derived extracellular vesicle-packaged WNTs rescue intestinal stem cells and enhance survival after radiation injury. Nat. Commun. *7*, 13096.

Sancho, E., Batlle, E., and Clevers, H. (2003). Live and let die in the intestinal epithelium. Curr. Opin. Cell Biol. *15*, 763–770.

Sangiorgi, E., and Capecchi, M.R. (2008). Bmi1 is expressed in vivo in intestinal stem cells. Nat. Genet. *40*, 915–920.

Snippert, H.J., van der Flier, L.G., Sato, T., van Es, J.H., van den Born, M., Kroon-Veenboer, C., Barker, N., Klein, A.M., van Rheenen, J., Simons, B.D., and Clevers, H. (2010). Intestinal crypt homeostasis results from neutral competition between symmetrically dividing Lgr5 stem cells. Cell *143*, 134–144.

Takeda, N., Jain, R., LeBoeuf, M.R., Wang, Q., Lu, M.M., and Epstein, J.A. (2011). Interconversion between intestinal stem cell populations in distinct niches. Science *334*, 1420–1424.

Taniguchi, C.M., Miao, Y.R., Diep, A.N., Wu, C., Rankin, E.B., Atwood, T.F., Xing, L., and Giaccia, A.J. (2014). PHD inhibition mitigates and protects against radiation-induced gastrointestinal toxicity via HIF2. Sci. Transl. Med. *6*, 236ra64.

Tata, P.R., Mou, H., Pardo-Saganta, A., Zhao, R., Prabhu, M., Law, B.M., Vinarsky, V., Cho, J.L., Breton, S., Sahay, A., et al. (2013). Dedifferentiation of committed epithelial cells into stem cells in vivo. Nature *503*, 218–223.

Tetteh, P.W., Basak, O., Farin, H.F., Wiebrands, K., Kretzschmar, K., Begthel, H., van den Born, M., Korving, J., de Sauvage, F., van Es, J.H., et al. (2016). Replacement of lost Lgr5-positive stem cells through plasticity of their enterocyte-lineage daughters. Cell Stem Cell *18*, 203–213.

Tian, H., Biehs, B., Warming, S., Leong, K.G., Rangell, L., Klein, O.D., and de Sauvage, F.J. (2011). A reserve stem cell population in small intestine renders Lgr5-positive cells dispensable. Nature *478*, 255–259.

Tsukiyama, T., and Yamaguchi, T.P. (2012). Mice lacking Wnt2b are viable and display a postnatal olfactory bulb phenotype. Neurosci. Lett. *512*, 48–52.

Valenta, T., Degirmenci, B., Moor, A.E., Herr, P., Zimmerli, D., Moor, M.B., Hausmann, G., Cantù, C., Aguet, M., and Basler, K. (2016). Wnt ligands secreted by subepithelial mesenchymal cells are essential for the survival of intestinal stem cells and gut homeostasis. Cell Rep. *15*, 911–918.

van Es, J.H., Sato, T., van de Wetering, M., Lyubimova, A., Yee Nee, A.N., Gregorieff, A., Sasaki, N., Zeinstra, L., van den Born, M., Korving, J., et al. (2012). Dll1+ secretory progenitor cells revert to stem cells upon crypt damage. Nat. Cell Biol. *14*, 1099–1104.

Xie, L., Xue, X., Taylor, M., Ramakrishnan, S.K., Nagaoka, K., Hao, C., Gonzalez, F.J., and Shah, Y.M. (2014). Hypoxia-inducible factor/MAZ-dependent induction of caveolin-1 regulates colon permeability through suppression of occludin, leading to hypoxia-induced inflammation. Mol. Cell. Biol. *34*, 3013–3023.

Yan, K.S., Chia, L.A., Li, X., Ootani, A., Su, J., Lee, J.Y., Su, N., Luo, Y., Heilshorn, S.C., Amieva, M.R., et al. (2012). The intestinal stem cell markers Bmi1 and Lgr5 identify two functionally distinct populations. Proc. Natl. Acad. Sci. USA *109*, 466–471.

Zimmerer, T., Böcker, U., Wenz, F., and Singer, M.V. (2008). Medical prevention and treatment of acute and chronic radiation induced enteritis–is there any proven therapy? A short review. Z. Gastroenterol. *46*, 441–448.

Cell Reports, Volume *21*

Supplemental Information

Quiescence Exit of Tert^{+} Stem Cells by Wnt/β-Catenin Is Indispensable for Intestinal Regeneration

Han Na Suh, Moon Jong Kim, Youn-Sang Jung, Esther M. Lien, Sohee Jun, and Jae-Il Park

Supplemental Figures

Supplemental Tables

Supplemental Experimental Procedures

SUPPLEMENTAL FIGURES

Figure S1. Characterization of Tert+ cells in the small intestine (Related to Figure 1)

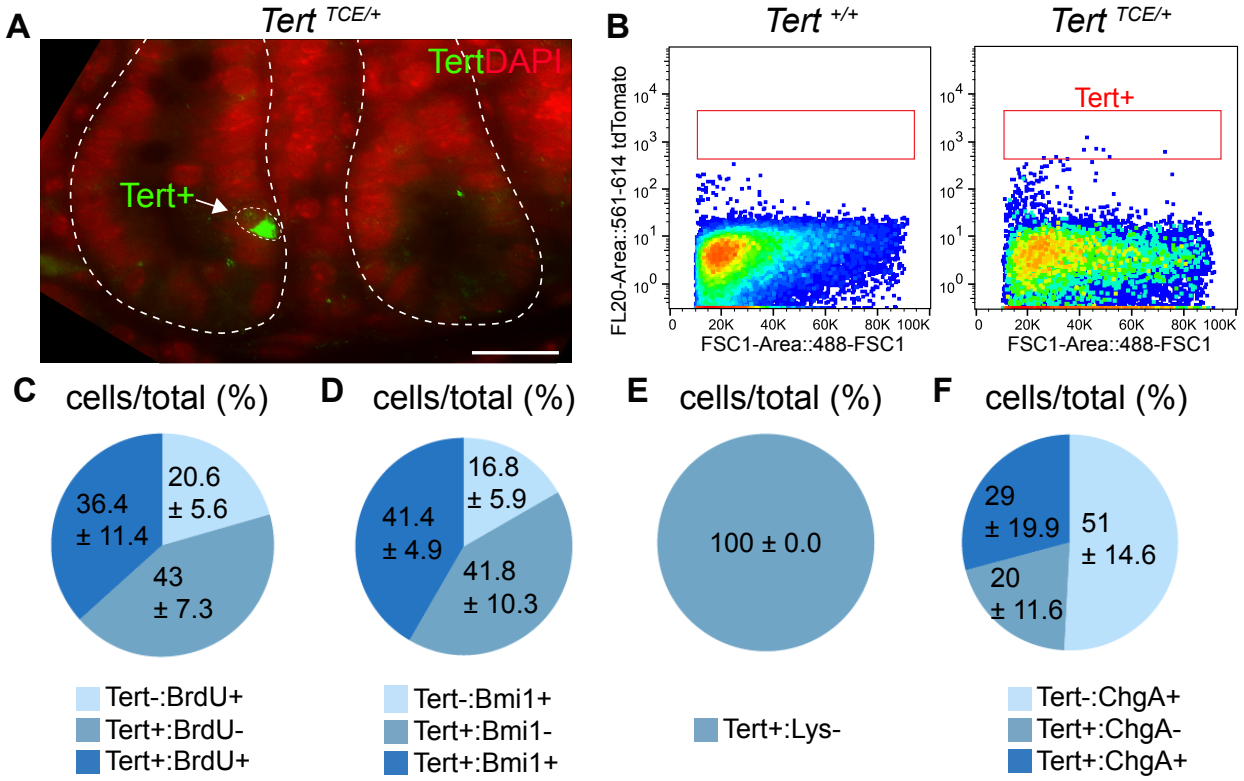

(A) Location of Tert+ cell in the crypts. Tert+ cells are rare (1 Tert+ cell per 120.5 ± 26.50 crypts).

(B) Assessment of Tert+ cell population in the small intestine.

Cells isolated from *Tert*$^{TCE/+}$ mice were quantified based on tdTomato fluorescence. Cells from *Tert*$^{+/+}$ mice were used as a negative control for gating. Quantitative analysis of Tert+ cells by FACS.

(C-F) Quantification graph of Figure 1F (**C**); Figure 1K (**D**); Figure 1L (**E**); Figure 1M (**F**).

Figure S2. IR-induced intestinal damage and regeneration (Related to Figure 2)

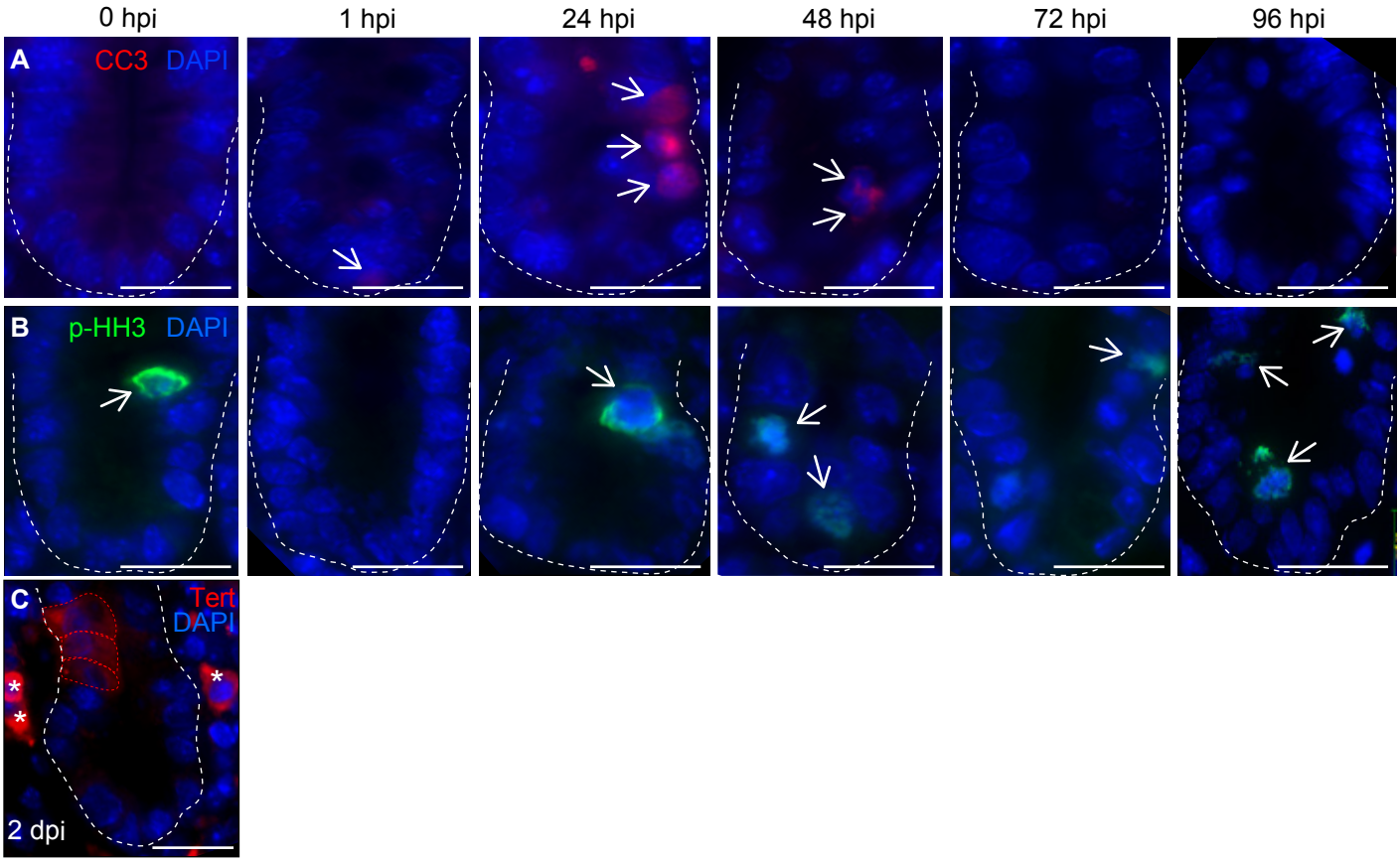

(A, B) WBI (10 Gy)-induced intestinal damage and regeneration.

Apoptosis (cleaved caspase 3) (**A**); mitosis (phospho-histone H3) (**B**). Arrows indicate the positive cells of each antibody. Hpi: hours post injury. Scale bars=20μm. The representative images are shown; N≥3.

(C) Expansion of Tert+ cells during regeneration. Tert+ cells rebuild the damaged intestinal epithelial at 2 dpi. Asterisk: non-specific signal. Scale bars=20μm.

Figure S3. Impaired intestinal regeneration by Tert+ cell ablation (Related to Figure 3)

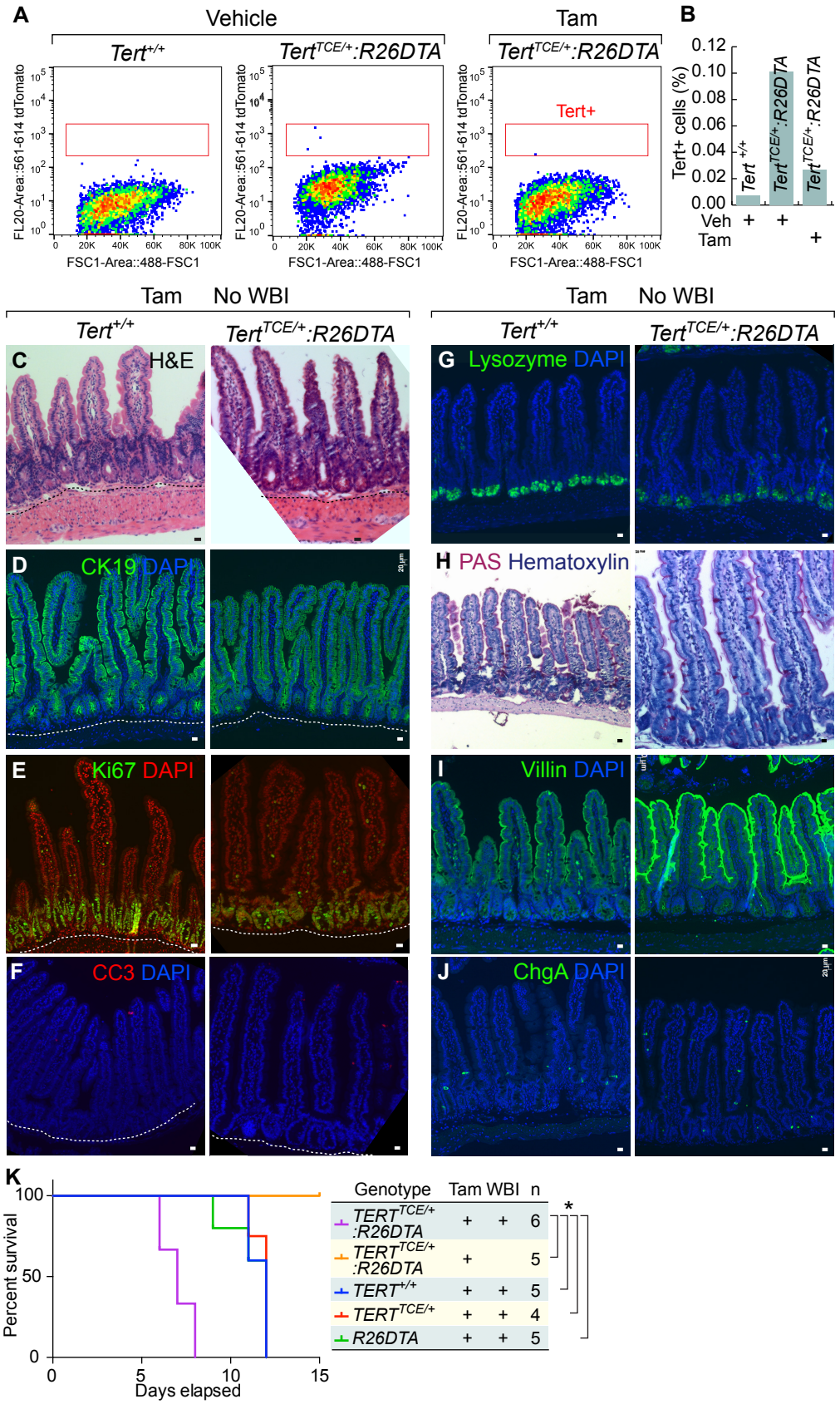

(A, B) Confirmation of Tert+ cell ablation after Tam treatment.

Tert$^{TCE/+}$:*Rosa26DTA* mice were administered by Vehicle (cone oil) or Tam (50 mg/kg, 5 times, 1 day interval). Tert+ cells were then quantified by FACS (**A**). Quantification graph (**B**). Tam treatment removed about 70% Tert+ cells in *Tert*$^{TCE/+}$:*Rosa26DTA* mice.

(C-J) No defect of intestinal epithelium after Tert+ cell ablation in homeostasis. H&E staining (**C**); epithelial structure (cytokeratin 19; CK19) (**D**); proliferation (Ki67) (**E**); apoptosis (CC3) (**F**); lysozyme (**G**); PAS (**H**); villin (**I**); chromogranin A (**J**). Scale bars=20μm; dot lines indicate the basal membranes below crypts. The representative images are shown; N≥3. Of note, in the absence of tissue injury (irradiation), Tert+ cell ablated mice (*Tert*$^{TCE/+}$*:Rosa26DTA*) were viable without any discernible phenotype.

(**K**) Kaplan Meier survival graph. *Tert*$^{TCE/+}$*:Rosa26DTA* treated with Tam and WBI showed the early lethality compared to *Tert*$^{+/+}$*, Tert*$^{TCE/+}$*,* and *Rosa26DTA*. Asterisks (*)=P<0.05.

Figure S4. Defects in intestinal regeneration by Tert+ cell ablation (Related to Figure 3)

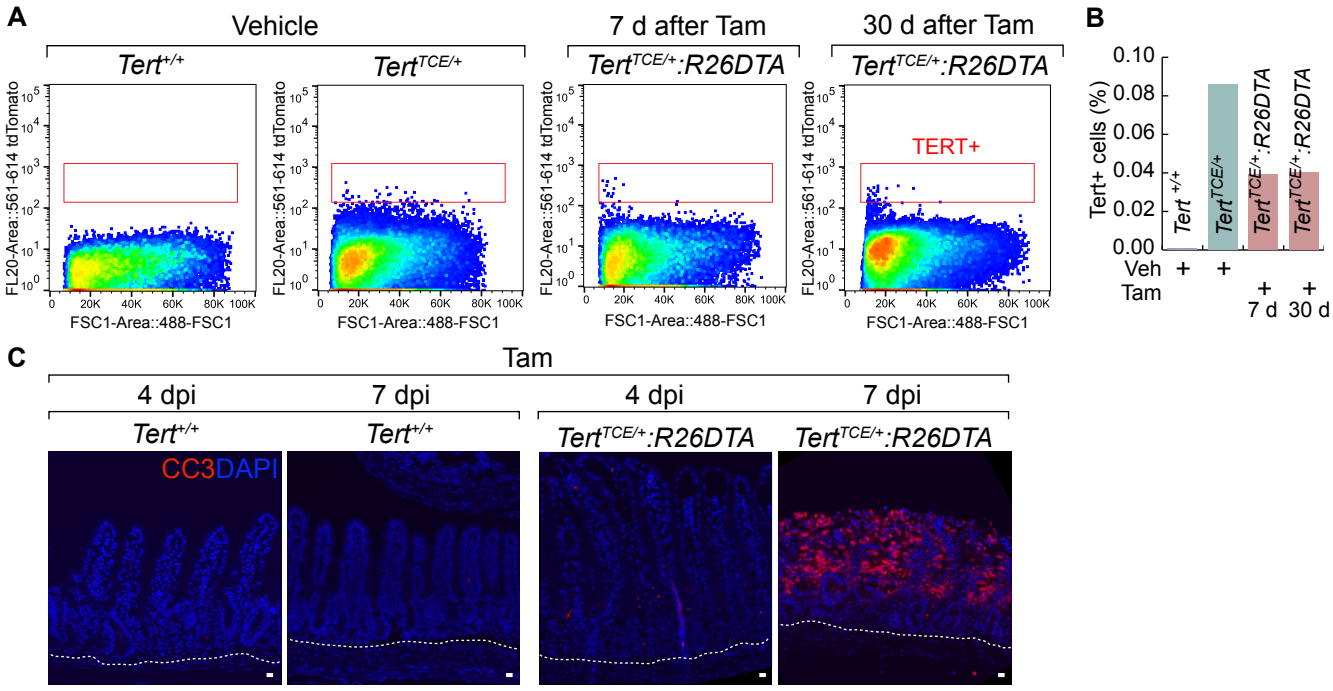

(A, B) No *de novo* generation of Tert+ cells after Tert+ cell ablation. *Tert*$^{TCE/+}$:*Rosa26DTA* mice were treated with Tam (50 mg/kg, 5 times, 1 day interval). 7 or 30 days after treatment, Tert+ cells were quantified by FACS (**A**). Quantification graph (**B**). *Tert*$^{TCE/+}$ mice were used as a positive control and *Tert*$^{+/+}$ mice were used as a negative control.

(C) Impaired intestinal regeneration by Tert+ cell ablation. Cleaved caspase-3 (CC3). Scale bars=20μm; dot lines indicate the basal membranes below crypts. The representative images are shown; N≥3.

Figure S5. Identification of Wnt ligands associated with intestinal regeneration (Related to Figure 4)

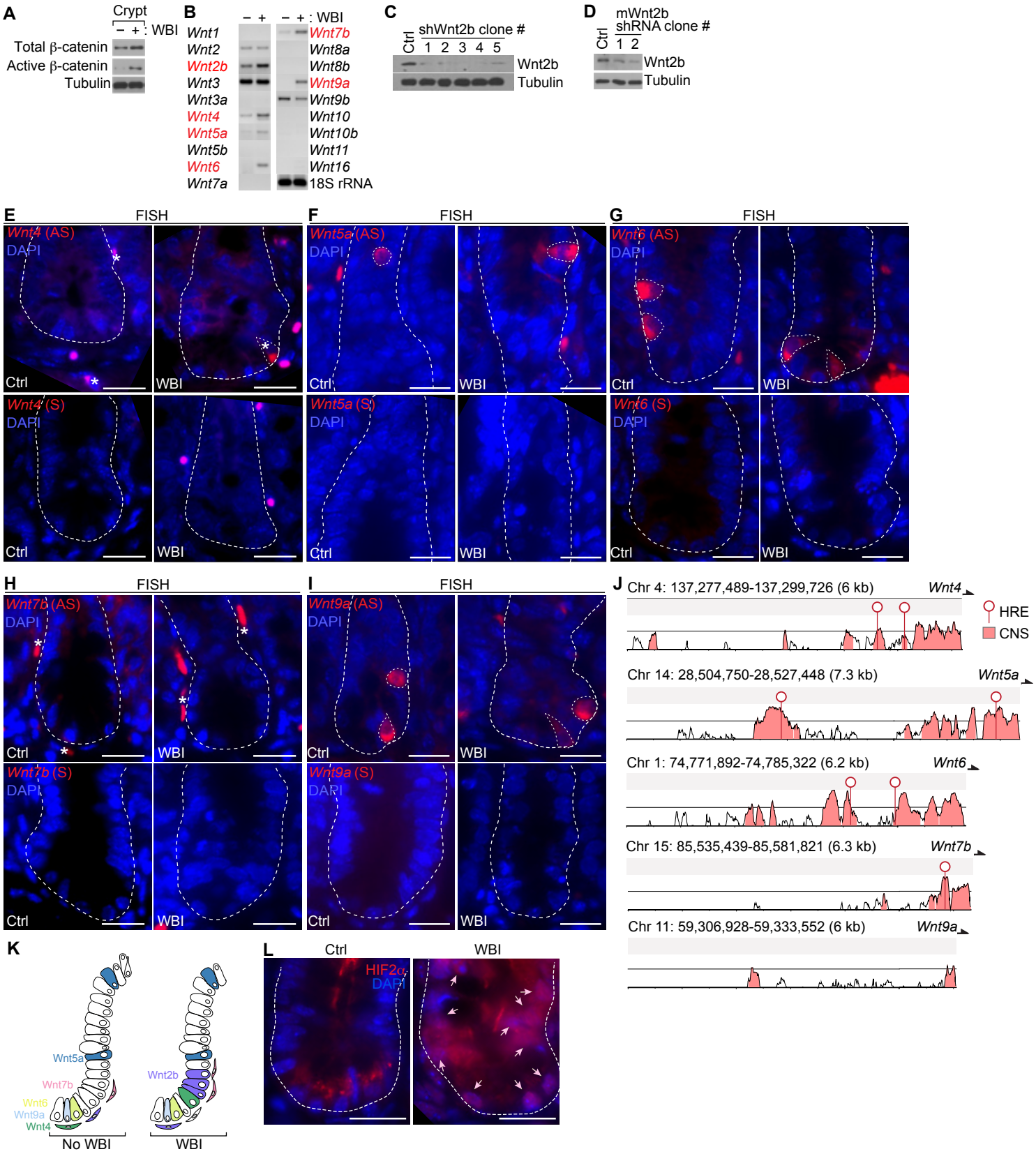

(A) Expression of β-catenin in the crypt after IR(10 Gy, 24 hpi). Both total β-catenin and active β-catenin were upregulated by IR.

(B) Expression of nineteen Wnt ligands in the crypt after IR (10 Gy, 24 hpi). The expression of *Wnt2b, Wnt4, Wnt5a, Wnt6, Wnt7b*, and *Wnt9a* mRNA was upregulated by IR.

(C) Depletion of endogenous Wnt2b using shRNAs. HCT116 cells were transduced with lentiviruses encoding shRNAs against Wnt2b (five clones; #1~#5) and analyzed for Wnt2b Western blot assays.

(D) Depletion of endogenous Wnt2b using mouse shRNAs. NIH/3T3 cells were transduced with lentiviruses encoding shRNAs against Wnt2b (two clones; #1~#2) and analyzed for Wnt2b Western blot assays.

(E-I) FISH for *Wnt4* (**E**), *Wnt5a* (**F**), *Wnt6* (**G**), *Wnt7b* (**H**), and *Wnt9a* (**I**) expression by WBI (10 Gy, 24 hpi). AS: antisense; S: sense; scale bars=20μm; asterisks: Wnt4+ cells (mesenchymal or epithelial), Wnt7b+ cells (mesenchymal). Among the six Wnt ligands examined, we selected *Wnt2b* to further study how IR activates Wnt/β-catenin signaling.

(J) Wnt ligand (Wnt4, Wnt5a, Wnt6, Wnt7b, and Wnt9a) promoter analysis for hypoxia response element (HRE). Conserved non-coding sequence (CNS); arrow indicates the transcription start site.

(K) Illustration of Wnt ligands localization and expression pattern during homeostasis and regeneration.

(L) Nuclear translocation of HIF2α after IR (10 Gy, 24 hpi). In addition to HIF1α (Figure 4M), HIF2α also showed nuclear translocation by IR. Scale bars=20mm.

Figure S6. β-catenin CKO in Tert+ cells (Related to Figure 5)

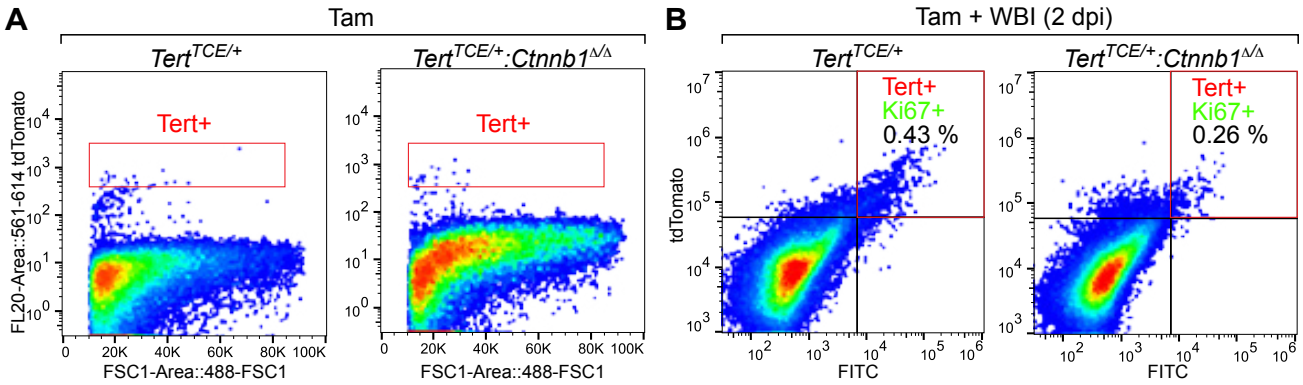

(A) Representative FACS plots of Figure 5N. β-catenin CKO in Tert+ cells did not affect the quantity of Tert+ cells in the small intestine.

(B) Representative FACS plots of Figure 5O. β-catenin CKO in Tert+ cells decreased the number of proliferative Tert+ cells (Tert+:Ki67+) upon WBI.

The representative images are shown; N≥3.

SUPPLEMENTAL TABLES

Table S1. Primer sequence information (Related to Figures 1, 2, 4, and 5)

Gene	**Forward (5' to 3')**	**Reverse (5' to 3')**
Tert	TGGGTCTC CCTGTACCAAAT	GGCCTGTAACTAGCGGACACA
Bmi1	TGATTCTGGTTCGATGC	TGGCTCGCATTCATTTTATG
Dll1	TGAGCCAGTCTTTCCTTGAA	AGACCCGAAGTGCCTTTGTA
Krt19	GGGGGTTCAGTACGCATTGG	GAGGACGAGGTCACGAAGC
Lrig1	TTGAGGACTTGACGAATCTGC	CTTGTTGTGCTGCAAAAAGAGAG
Alpi	CATGGACCGCTTCCCATA	CTTGCACTGTCTGGAACCTG
Lgr5	ACCTGTGGGTAGATGACAATGC	TCCAAAGGGGTAGTCTGCTAT
Lig4	AGTCTGCAAAGGGGACATGA	CTTTCTCTTCCACCATGGCT
Xrcc5	TGTCCAACGACAGGTATTTTCG	AAGGGCATTATCAGTGCCATC
Xrcc4	CTTGCTTCTGAACCCAACGTA	TGGCCGTCAGTAAGTGTAATAAC
Blm	AGCGACACTCAGCCAGAAAAC	GCCTCAGACACGTTCACATCTT
Rpa1	GGGACACAGTCCAAAGTGGTG	GACACGGGCACAAATAGTCCA
Rad51c	CGGGAGTTGGTGGGTTATCC	CCGGCACATCTTGGTTTATTTGT
p19	TCAGGAGCTCCAAAGCAACT	TTCTTCATCGGGAGCTGGT
p107	AGGGAGAAGTTATACACTGGCT	CCCTTTCCCACAGTAGGAATGA
trp53bp2	AGTAAAGGCTCTAAAGCTCACCC	GTAAGAGGTCGGCATTGGAAG
p130	AACTTCCCCATGATTAGCCATG	GGTTAGAACACTGAAGGGCATTT
trp53ip2	GCGCCCTCCTTGATGGATG	TCCTCCAGCGGATTGCTCT
p21	CCTGGTGATGTCCGACCTG	CCATGAGCGCATCGCAATC
Rb1	TGCATCTTTATCGCAGCAGTT	GTTCACACGTCCGTTCTAATTTG

Ccne1	GTGGCTCCGACCTTTCAGTC	CACAGTCTTGTCATTCTTGGCA
p16	CAAAGTGACAGATGCTCCAATCC	TTTTCCTTCTACGGCTCGTTTT
Ccnd1	GCGTACCCTGACACCAATCTC	CTCCTCTTCGCACTTCTGCTC
CD133	TCGTACTGGTGGCTGGGTGGC	ACCACAAGGATCATCAATATC
Axin2	TGCATCTCTCTCTGGAGGTG	TATGTCTTTGCACCAGCCAC
CD44	AGCGGCAGGTTACATTCAAA	CAAGTTTTGGTGGCACACAG
Ctgf	AGCCTCAAACTCCAAACACC	CAACAGGGATTTGACCAC
Glil1	ACCACCCTACCTCTGTCTATTC	TTCAGACCATTGCCCATCAC
Hes1	GGTATTTCCCCAACACGGT	GGCAGACATTCTGGAAATGA
Ptprq	CGGAGGTTACTGGAACCGTG	CAGGGTCCCCACATAGCCT
Nestin	CTGCAGGCCACTGAAAAGTT	GACCCTGCTTCTCCTGCTC
ChgA	GCAGAGGACCAGGAGCTAGA	CAGGGGCTGAGAACAAGAGA
ChgB	ACAGGAAGAAGGCAGACGAA	TCCTTCAGTGAAAGGCTCGT
Mmp7	CCCGGTACTGTGATGTACCC	AATGGAGGACCCAGTGAGTG
Wnt1	TCTTTGGCCGAGAGTTCGTG	AGAGAACACGGTCGTTCGC
Wnt2	ATCTCTTCAGCTGGCGTTGT	AGCCAGCATGTCCTCAGAGT
Wnt2b	CACGTCACAACAATGAGGCT	TCGGCACCTTGAAGTACGTG
Wnt3	TGGAACTGTACCACCATAGAT	ACACCAGCCGAGGCCATG
Wnt3a	ACCGTCACAACAATGACGCT	TCGGCACCTTGAAGTACGTG
Wnt4	AACGGAACCTTGAGGTGATG	GGACGTCCACAAAGGACTGT
Wnt5a	CACGCTATACCAACTCCTCTGC	AATATTCCAATGGGGTTCTTC
Wnt5b	GCCGCGGATGAGGAGTG	GCCTCAACCCATCCCAATGC
Wnt6	CGGAGACGATGTGGACTT	GGAACCCGAAAGCCCATG
Wnt7a	ATCAAGCAGAATGCCCGGAC	TAGCTCTCGGAACTGTGGCA

Wnt7b	ACTCCGAGTAGGGAGTCGAGA	GCGACGAGAAAAGTCGATGC
Wnt8a	TGGGAACGGTGGAATTGTCC	GCAGAGCGGATGGCATGAAT
Wnt8b	GTGGACTTCGAAGCGCTAAC	TTACACGTGCGTTTCATGGT
Wnt9a	TGCTTTCCTCTACGCCATCT	TATCACCTTCACACCCACGA
Wnt9b	GTGTGGTGACAATCTGAAG	GTGTGGTGACAATCTGAAG
Wnt10a	GCTTCGGAGAACGCTTCTCT	ATTTGCACTTACGCCGCATG
Wnt10b	GGAAGGGTAGTGGTGAGCAA	CACTTCCGCTTCAGGTTTTC
Wnt11	GTTCTCCGTGATTGCAGGCG	TTGCGTCTGATTCAGTGCCA
Wnt16	CTGTGACACCACCTTGCAGA	CAGGTTTTCACAGCACAGGA
18S rRNA	AAGTCCCTGCCCTTTGTACACA	GATCCGAGGGCCTCACTAAAC
Wnt2b i	CTAGTCCCAGTGTGGGGAAA	TTCTCGGTGTCTGGCTTTCT
Wnt2b ii	CTGGGGACATTTGCTCTGTT	TGGGGTTCTTGGCTTGTTAC
Wnt2b iii	GGAACACAGCCTCTTCTGG	CACAGATGCTCGGCTATTGA
Wnt2b iv	GGGCACTCTGCTCCATTTAG	CACGGGGAATGCTACAAAGT
Wnt2b v	AAAGCACCAAGGTGGACAAG	TGCGCTTCTAGGAAACTGGT

Table S2. Antibody information for IHC (Related to Figures 1-5)

Protein; Company (cat #); Dilution

BrdU and CldU; Abcam (ab6326); 1/100

Ki67; Abcam (ab1667); 1/100

IdU; Abcam (ab181664); 1/100

Bmi1; Abcam (ab14389); 1/100

p-γH2AX; Cell signaling (#9718);1/200

Cleaved Capase 3; Cell signaling (#9664s); 1/200

p-HH3; Cell signaling (#9706); 1/200

Lysozyme; Abcam (ab108508); 1/400

Villin; Thermo (PA5-22072); 1/200

ChgA; Abcam (ab15160); 1/200

CK19; Abcam (ab133496); 1/200

β-catenin; Cell signaling (#9587s); 1/250

β-galactosidase (LacZ); Abcam (ab4761); 1/200

CD44; BD Biosciences (550538); 1/100

Cyclin D1; Cell signaling (#2978S); 1/50

8-oxo-dG; Abcam (ab62623); 1/200

HIF1α; Abcam (ab1); 1/100

HIF2α; Abcam (ab199); 1/100

C-Myc; Santa Cruz (sc 764); 1/80

SUPPLEMENTAL EXPERIMENTAL PROCEDURES

Crypt and single cell organoids

For crypt organoids, intestinal crypts were isolated. For single cell isolation, crypts were digested with Accumax (Stem cell technology 07921) for 5 min and single cells were collected through 70 μm (BD 087712) and 40 μm (BD 087711) cell strainers. Crypts or single cells were then suspended in growth factor-reduced Matrigel (Corning 356231). After polymerization, organoid culture medium composed of 50% conditioned medium from L-WRN cells (ATCC® CRL-3276™) (1:1 dilution with Advanced DMDM/F12) containing 1 mM *N*-acetyl cysteine, B27 supplement, N2 supplement, 50 ng/ml mouse EGF, 10 μM Y-27632 was overlayed.

Organoid lentiviral infection

Single cells isolated from crypts of *C57BL/6* were incubated with media containing lentiviruses expressing mouse Wnt2b shRNAs (Dharmacon clone ID V3LMM_505459, V3LMM_505462), 7 μg/ml polybrene, 1 mM Jagged-1 peptide, and 10 μM Y-27632 for 2 h at 37 °C. Infected cells were then suspended with Matrigel, seeded in 24 well culture plates, and overlayed with organoid culture medium. Next day, fresh organoid culture medium with selection antibiotic (puromycin, 2 μg/ml) was added to the organoids. Survival of GFP+ cells was considered as infected cells. GFP shRNA (Sigma SHC005) was used as a negative control.

X-gal staining

Axin2-LacZ mice were treated with 10 Gy WBI and intestine was collected for 5-bromo-4-chloro-3-indolyl-β-D-galacto-pyranoside (X-gal) staining (Sigma GALS-1KT). Intestine was fixed with 2% formaldehyde containing 0.2% glutaraldehyde for 10 min at room temperature, rinsed with PBS, and incubated with Staining solution [2 mM $MgCl_2$, 4 mM $K_3Fe(CN)_6$, 4 mM $K_4Fe(CN)_6$, 1 mg/ml X-gal] for 2 h at 37°C. Stained intestine was washed, post-fixed, and analyzed. Nuclear fast red was used for nuclear counterstaining.

Cell line

CCD 841 CoN cell line was acquired from ATCC (CRL-1790™) and maintained with Eagle's Minimum Essential Medium (ATCC® 30-2003) containing 10% fetal bovine serum. CCD 841 CoN is originated from 21 weeks gestation female fetus. NIH/3T3 cell line was acquired from ATCC (CRL-1658™) and maintained with Dulbecco's Modified Eagle's Medium containing 10% fetal bovine serum.

Isolation of mesenchymal and epithelial cells

Mouse intestine was collected, cut transversely, and minced into small pieces in cold PBS. Tissue was incubated in 5 mM EDTA for 1 h at 4°C on orbital shaker. After incubation, tissues were passed through a 100 μm cell strainer. Flow thorough (epithelium) and remained pieces on the strainer (mesenchyme) were collected for further analysis.

Detection of intracellular reactive oxygen species

CCD841CoN was cultured on coverglass until 50% confluent. After 10 Gy IR, cells were incubated with cell-permeable 2',7'-dichlorodihydrofluorescein diacetate (1 μM, H_2DCFDA; Thermo) for 30 min. Cells were then washed twice with PBS, stained with Hoechst 33342 for nucleus counterstaining, and photographed using fluorescence microscope (Zeiss; AxioVision).

Immunohistochemistry

Mouse intestinal tissues were fixed in 10% neutral buffered formalin overnight, made into Swiss role, and embedded in paraffin. Tissue samples were then sectioned (5 μm), deparaffinized, processed for antigen retrieval, blocked, incubated with primary antibody, and fluorescence or peroxidase-conjugated secondary antibody. Samples were mounted and photographed using a microscope (Zeiss; AxioVision). For comparison among the experiment groups, images were captured with the same exposure time. For peroxidase-conjugated secondary antibody, 3,3'-Diaminobenzidine (DAB) substrate was used, followed by hematoxylin for nuclear counterstaining. All antibody information is listed in Supplemental Table2.

Immunofluorescence staining

Cells grown on coverglass were fixed with 4% paraformaldehyde, permeabilized with 0.01% Triton X-100 in PBS, blocked with 5% BSA, incubated with primary antibody (HIF-1α) and fluorescence-conjugated secondary antibody. Cells were stained with Hoechst 33342 for nuclear counterstaining and photographed using a fluorescence microscope (Zeiss; AxioVision). For comparison, images were captured under the same exposure time. Representative images were shown.